NAVAL POSTGRADUATE SCHOOL
Monterey, California

THESIS

ION GUN OPERATIONS AT HIGH ALTITUDES

by

Paul W Werner

June 1988

Thesis Advisor: Richard C. Olsen

SECURITY CLASSIFICATION OF THIS PAGE A196965

REPORT DOCUMENTATION PAGE

1a. REPORT SECURITY CLASSIFICATION UNCLASSIFIED	1b RESTRICTIVE MARKINGS
2a. SECURITY CLASSIFICATION AUTHORITY	3 DISTRIBUTION / AVAILABILITY OF REPORT APPROVED FOR PUBLIC RELEASE DISTRIBUTION IS UNLIMITED
2b. DECLASSIFICATION / DOWNGRADING SCHEDULE	
4. PERFORMING ORGANIZATION REPORT NUMBER(S)	5 MONITORING ORGANIZATION REPORT NUMBER(S)
6a. NAME OF PERFORMING ORGANIZATION NAVAL POSTGRADUATE SCHOOL 6b OFFICE SYMBOL (If applicable) CODE 61	7a. NAME OF MONITORING ORGANIZATION NAVAL POSTGRADUATE SCHOOL
6c. ADDRESS (City, State, and ZIP Code) MONTEREY, CALIFORNIA 93943-5000	7b. ADDRESS (City, State, and ZIP Code) MONTEREY, CALIFORNIA 93943-5000
8a. NAME OF FUNDING / SPONSORING ORGANIZATION 8b. OFFICE SYMBOL (If applicable)	9. PROCUREMENT INSTRUMENT IDENTIFICATION NUMBER
8c. ADDRESS (City, State, and ZIP Code)	10. SOURCE OF FUNDING NUMBERS PROGRAM ELEMENT NO. / PROJECT NO. / TASK NO / WORK UNIT ACCESSION NO

11. TITLE (Include Security Classification)

ION GUN OPERATIONS AT HIGH ALTITUDES

12. PERSONAL AUTHOR(S) WERNER, PAUL W

13a. TYPE OF REPORT	13b. TIME COVERED	14. DATE OF REPORT (Year, Month, Day)	15 PAGE COUNT
MASTER'S THESIS	FROM _____ TO _____	1988 JUNE	98

16. SUPPLEMENTARY NOTATION

THE VIEWS EXPRESSED IN THIS THESIS ARE THOSE OF THE AUTHOR AND DO NOT REFLECT THE OFFICIAL POLICY OR POSITION OF THE DEPARTMENT OF DEFENSE OR THE U.S. GOVERNMENT

17. COSATI CODES			18. SUBJECT TERMS (Continue on reverse if necessary and identify by block number)
FIELD	GROUP	SUB-GROUP	ION GUN, SPACECRAFT CHARGING, SCATHA

19. ABSTRACT (Continue on reverse if necessary and identify by block number)

EXPERIMENTS IN CHARGE CONTROL WERE CONDUCTED ON THE P78-2 (SCATHA) SATELLITE AS PART OF A JOINT AIR FORCE/NASA PROGRAM ON SPACECRAFT CHARGING AT HIGH ALTITUDES. EXPERIMENTS WITH THE SCATHA ION GUN WERE MONITORED BY CHARGED PARTICLE DETECTORS AND THE ELECTRIC FIELD EXPERIMENT. IT WAS FOUND THAT THE ELECTRIC FIELD EXPERIMENT COULD BE USED TO MEASURE SATELLITE POTENTIAL DURING ION BEAM EMISSION IN SUNLIGHT AND ECLIPSE. UNNEUTRALIZED ION BEAM EMISSION IN HIGH ENERGY (1 - 2 KeV) AND HIGH CURRENT (1-2 mA) MODES RESULTED IN THE SATELLITE MOMENTARILY CHARGING TO A NEGATIVE POTENTIAL NEAR THE MAGNITUDE OF THE BEAM VOLTAGE AND THEN RISING TO SOME LESS NEGATIVE VALUE, TYPICALLY -500 TO -800 V. THE NET EMITTED CURRENT WAS APPARENTLY LIMITED BY THE FORMATION OF A VIRTUAL ANODE. LOW CURRENT (20-30 μA), HIGH VOLTAGE (1 kV) RESULTED IN -10 TO -50 V SATELLITE POTENTIALS. TRICKLE MODE (20-80 μA, NO ACCEL VOLTAGE) OPERATIONS RESULTED IN SATELLITE POTENTIALS NEAR ZERO VOLTS. IN SUNLIGHT THE SPACE CRAFT POTENTIAL EXHIBITED A SPIN MODULATION, ATTRIBUTED TO VARIATIONS IN THE NEUTRALIZATION OF THE BEAM AS IT PASSED THROUGH THE PHOTOELECTRON CLOUD. RAPID FLUCTUATIONS OF THE SPACE CRAFT POTENTIAL OCCURED WHICH MAY BE EXPLAINED QUALITATIVELY BY SPACE CHARGE INSTABILITES

20. DISTRIBUTION / AVAILABILITY OF ABSTRACT	21. ABSTRACT SECURITY CLASSIFICATION
☒ UNCLASSIFIED/UNLIMITED ☐ SAME AS RPT ☐ DTIC USERS	UNCLASSIFIED
22a. NAME OF RESPONSIBLE INDIVIDUAL R. C. OLSEN	22b TELEPHONE (Include Area Code) (408) 646-2019 22c. OFFICE SYMBOL 61 OS

DD FORM 1473, 84 MAR 83 APR edition may be used until exhausted. All other editions are obsolete

SECURITY CLASSIFICATION OF THIS PAGE

U.S. Government Printing Office: 1986—606-24

Approved for public release: distribution is unlimited.

Ion Gun Operations at High Altitudes

by

Paul W. Werner
Lieutenant, United States Navy
B. S., University of Utah, 1980

Submitted in partial fulfillment of the
requirements for the degree of

MASTER OF SCIENCE IN PHYSICS

from the

NAVAL POSTGRADUATE SCHOOL
June 1988

Author: Paul W. Werner
Paul W. Werner

Approved by: Richard Chris Olsen
Richard C. Olsen, Thesis Advisor

Otto Heinz
O. Heinz, Second Reader

K.E. Woehler, Chairman, Department of Physics

Gordon E. Schacher, Dean of Science
and Engineering

ABSTRACT

Experiments in charge control were conducted on the P78-2 (SCATHA) satellite as part of a joint Air Force/NASA program on spacecraft charging at high altitudes. Experiments with the SCATHA ion gun were monitored by charged particle detectors and the electric field experiment. It was found that the electric field experiment could be used to measure satellite potential during ion beam emission in sunlight and eclipse. Unneutralized ion beam emission in high energy (1-2 KeV) and high current (1-2 mA) modes resulted in the satellite momentarily charging to a negative potential near the magnitude of the beam voltage and then rising to some less negative value, typically -500 to -800 V. The net emitted current was apparently limited by the formation of a virtual anode. Low current (20-30 μA), high voltage (1 kV) resulted in -10 to -50 V satellite potentials. Trickle mode (20-80 μA, no accel voltage) operations resulted in satellite potentials near zero Volts. In sunlight the spacecraft potential exhibited a spin modulation, attributed to variations in the neutralization of the beam as it passed through the photoelectron cloud. Rapid fluctuations of the spacecraft potential occured which may be explained qualitatively by space-charge instabilities.

TABLE OF CONTENTS

ACKNOWLEDGMENT

The author expresses his appreciation to Professor R. C. Olsen, whose unwavering patience and scholarly advice led him through the obstacles of research. Dr. Olsen's work on this project was supported by the Naval Postgraduate School Foundation research program and by NASA/Lewis Research Center.

The author also wishes to thank Dr. S. E. McIlwain and Dr. E. C. Whipple (UCSD) for providing support in analysis of the data; Ms. W. W. Li for help in processing the data; Dr. T. L. Aggson (NASA/GSFC), the PI for the SC10 experiment; and Mr. H. Cohen, the PI for the SC4 experiment.

I. INTRODUCTION AND BACKGROUND

A. INTRODUCTION

This thesis is concerned with the equilibrium and time dependent potentials of a spacecraft in the magnetosphere and the effect of active ion particle emission on them. An understanding of spacecraft charging is important because charging can directly affect satellite survival. Charging is also of great concern to space scientists studying the satellite environment primarily because of its effect on the measurement of ambient particles. This thesis is based on data collected by the UCSD particle detectors and the GSFC electric field monitors on the SCATHA satellite. The active ion emission was accomplished by the AFGL ion gun experiment.

The problem of spacecraft charging has been an ongoing concern since the early days of satellite flights (Whipple, 1965). With the advent of geosynchronous spacecraft, the observations showed the existence of even higher potentials, up to kilovolts in eclipse (DeForest, 1972). Potentials of this size can produce damaging electrostatic discharges which may result in spacecraft anomalies or malfunctions (McPherson et al., 1975). The remainder of this

introductory chapter presents the foundations and principles of charging and active spacecraft potential control.

B. PROBLEM OF SATELLITE CHARGING

Spacecraft charging to high levels at geosynchronous orbit was first reported by DeForest in 1972 (DeForest, 1972). Charging effects were identified by characteristic signatures in the charged particle data. Accelerated ambient ion fluxes result in a peak in the low-energy ion spectra at the spacecraft potential. Charging levels to tens of kilovolts negative were observed in eclipse and levels to several hundred volts negative were observed in sunlight (Gussenhoven and Mullen, 1983; Olsen and Purvis, 1983; Mullen et al., 1986). Satellite charging, in general, has not been a problem at low altitudes because of low plasma temperatures and high densities. Exceptions to this trend have recently been found in DMSP data (Yeh and Gussenhoven, 1987).

In addition to charging relative to the environment, the spacecraft may also differentially charge due to the various conducting and insulating characteristics of the different materials of which the spacecraft is composed. Differential charging sets up a "barrier" that traps electrons near the satellite and inhibits current flow. This may cause the satellite mainframe to charge more negatively than otherwise possible due to the environment alone.

Large spacecraft potentials give rise to the possibility of electrostatic discharges that could damage the spacecraft. Anomalies and malfunctions and negative charging events are strongly concentrated in the midnight to dawn local time sectors, as shown in Figure 1 (McPherson, 1975). These anomalies were generally logic upsets or switching failures that might be attributed to electrostatic discharges.

Because analysis of data from a satellite requires an accurate knowledge of the satellite potential and the existence of a large potential strongly affects charged particle measurements and satellite survival, there is strong incentive to understand the causes and methods of control of those potentials. These subjects also have important implications for the design of high-voltage spacecraft and the large-scale structures which are planned to be built in space in the near future.

C. HISTORY OF ACTIVE EXPERIMENTS

The first American experiment involving artificially generated positive ions was SERT I in 1964. This was a rocket test of a mercury ion thruster and successfully demonstrated thrust and beam neutralization. A plasma source which is used primarily as a means for spacecraft potential control is often called a "plasma contactor" or "plasma bridge". In November 1969 and August 1970, the Soviets

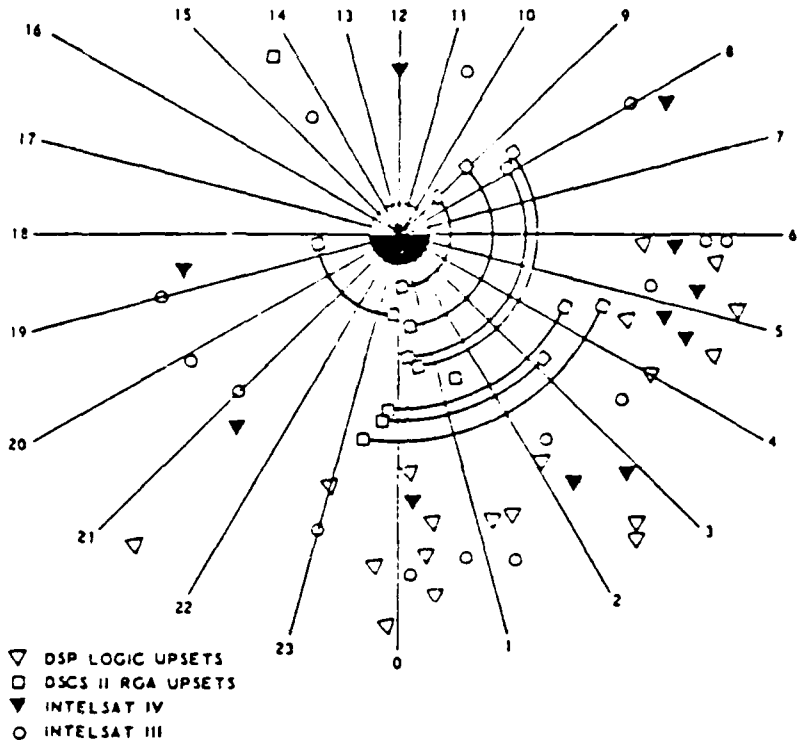

Figure 1. Occurrences of satellite anomalies plotted as a function of local time in geostationary orbit The radial distance is not significant.

launched two rockets containing ion engines in order to study engine system operations under near-natural conditions. The ion engines were part of automatic ionosphere space-flight laboratories and used surface ionization of cesium on tungsten. Also studied was the effect on neutralizer efficiency of neutralizers of different characteristics situated at different distances from the beam. (Gavrilov et al., 1973)

SERT II, launched on February 3, 1970, was the first successful orbital flight of an ion engine. It demonstrated that varying the potential of the neutralizer with respect to the spacecraft caused variations in the beam to spacecraft potential, and therefore the spacecraft potential with respect to the distant plasma. Plasma bridge neutralizers provided an electron current to neutralize the beam. (Jones et al., 1970)

ATS-4, -5, and -6 each carried a cesium ion thruster. ATS-4 and -5 both suffered malfunctions and complete testing of the ion engines was not possible. ATS-4, launched August 10, 1968, suffered a launch vehicle failure and entered a low altitude elliptical orbit. Limited testing indicated that the ion engine was working properly. (Hunter and Bartlett, 1969)

ATS-5 spun up in the wrong direction and at too high a spin rate (100 rpm) when ejected into its final orbit,

seriously limiting thruster operation. The limited operations with the ion engine were successful and indicated no change in the spacecraft potential, within the 50 eV low energy limit of the UCSD particle detectors. Electron emission experiments with the hot filament neutralizer in eclipse reduced large negative potentials to near zero but differential charging of the insulating surfaces ultimately suppressed electron emission. This reduced the effectiveness of the emitter in controlling the spacecraft potential. ATS-6 ion engine operation clamped the spacecraft potential to about -5 volts and suppressed differential charging. Operation of the plasma bridge neutralizer alone maintained the potential to within a few volts of the ambient plasma potential for all plasma conditions observed. ATS-6 provided evidence that a low energy plasma discharge can provide an effective means for controlling spacecraft potential. (Olsen, 1985)

The West German Porcupine rocket contained a Xenon ion gun which directed a 200 eV Xe+ ion beam perpendicular to the Earth's magnetic field. The dynamics of the plasma jet and associated wave processes were studied via an instrumented central payload and on subpayloads ejected from it. (Kintner and Kelley, 1981)

Most of the space experiments performed with energetic ions so far have used plasma beams rather than non-neutral

ion beams. Table 1 (Banks et al., 1987) gives a list of plasma beam space experiments since the beginning of 1975. The ATS satellites and SCATHA are not listed because their plasma sources were considered too small to be useful for ionospheric modification. Most of the experiments listed in the table used rockets. The exceptions are the Soviet 'Meteor' experiment, performed from a satellite, and the Japanese SEPAC experiment, part of the Spacelab-1 payload on the NASA Space Shuttle. The energies quoted are those of the positive ions.

The Araks payload had an electron gun as the main active device with the plasma source acting primarily as a source of neutralizing ions rather than a source of energetic ions. The plasma was ejected continuously and more or less perpendicular to the local magnetic field so that it would remain near the payload. This allowed the payload to more readily collect neutralizing electrons from the ambient ionosphere. The data are not clear on how successfully the potential was controlled. The plasma sources on ATS-6 and SCATHA were quite successful in this respect. The remaining experiments in the table are similar to the Porcupine experiment in that the plasma source was the main active device. In most cases the plasma source was operated in pulses and not continuously in order to observe the effects with the source active and with it switched off. The

scientific objective of most of these experiments was to study the propagation of plasma beams through the space plasma in the presence of the Earth's magnetic field. (Banks et al., 1987).

TABLE I

SPACE EXPERIMENTS WITH POSITIVE ION BEAMS, SINCE 1-1-75

Title	Date	Altitude	Ion	Energy	Current
ARAKS	(1) 1-26-75 (2) 2-15-75	(1) 190 km (2) 185 km	Caesum	50 eV	10 A
ARIEL	(1)10-29-77 (2)10-30-77 (3)11-30-78 (4)11-18-79	115-160 km 115-160 km 110-145 km 110-145 km	Barium unknown unknown Barium	unknown	unknown
METEOR	1977-79	850-900 km	Xenon	130 eV	unknown
AELITA	(1)10-06-78 (2)10-25-79	100-145 km	Lithium	4-10 eV	300 A
Porcupine	(1) 3-19-79 (2) 3-31-79	196-464 km 191-451 km	Xenon	200 eV	4 A
ARCS	(1) 1-27-80 (2)11-14-82	120-220 km 120-451 km	Argon	25 eV 33 eV	0.1 A
SEPAC	11-28-83	240 km	Argon	110 eV	1.6 kA
ARCS 3	2-10-85	129-406 km	Argon	200 eV	0.2 A

D. THEORY

A spacecraft in the magnetosphere is effectively a probe in a plasma. Elements which must be added to basic probe theory are the anisotropic current introduced by photoemission, secondary electron emission, and the addition of insulating surfaces to the probe so that it is no longer an equipotential surface.

In equilibrium, the magnitude of the potential is defined by the requirement that the currents to and from the satellite sum to zero. A non-zero sum is a net charging current, and the spacecraft will charge till it reaches equilibrium. A spacecraft will discharge and charge with two capacitive time constants. One is for the potential modulation of the mainframe or ground potential and the other the differential charging of the insulated surfaces. The major terms in the current balance equation are: ambient electrons, ambient ions, secondary electrons due to electron impact, secondary electrons due to ion impact, and photoelectrons. The environment and the surface of the satellite are therefore important because of the effects of ambient electrons and ions, photoelectrons, and secondary electrons. At geosynchronous altitudes, the high-energy electron current, that is, the current from that portion of the electron population with energies greater than about 30

KeV, drives the spacecraft frame potential in both sunlight and eclipse (Gussenhoven and Mullen, 1983).

Photocurrent is the major current from the spacecraft, the exact level of which depends on the work function of the irradiated material. Typical values in sunlight are 10-100 $\mu A/m^2$, one to two orders of magnitude larger than the next most important term, the ambient electron flux. Secondary emission is caused by the impact of primary particles with sufficiently high energy. The yield (the number of emitted electrons per incident electron) can exceed unity for primary particle energies of a few hundred eV. A spacecraft with an insulated surface is rarely equipotential because of the different secondary emission characteristics of its various surfaces. For an insulated surface in shadow, secondary electron emission due to primary electrons is particularly important since this is the term which determines if the surface will charge negatively.

At or near geosynchronous orbit, a satellite is usually in the plasmasphere or plasma sheet, two very different regimes. As the level of solar activity varies the boundaries move and the characteristics of the regions change. The plasmasphere, a cold (several eV) and dense (10-100 cm^{-3}) plasma, extends outward from its source, the ionosphere, and corotates with the Earth. The outer boundary is not well defined and varies with local time and magnetic

activity. The spacecraft is most likely to be in the plasmasphere between the hours of 1000 LT and 2000 LT. The plasmasphere may move completely inside geosynchronous orbit on some days following high magnetic activity. On other days following prolonged magnetic quiet, the plasmasphere may expand to envelope most of the geosynchronous orbit. The average position of the plasmapause shown in the equatorial plane of the magnetosphere is shown in Figure 2 (Chappell, 1974).

The plasma sheet begins where corotation effects are dominated by the cross-tail magnetospheric electric field. Densities in the plasma sheet are typically on the order of 1 cm^{-3} and temperatures for both ions and electrons typically exceed 10 KeV. Ambient currents are high in the plasma sheet and spacecraft charging is limited to periods when the vehicle is in the plasma sheet. The satellite is normally inside the plasmasheet between 2100 LT and 0900 LT.

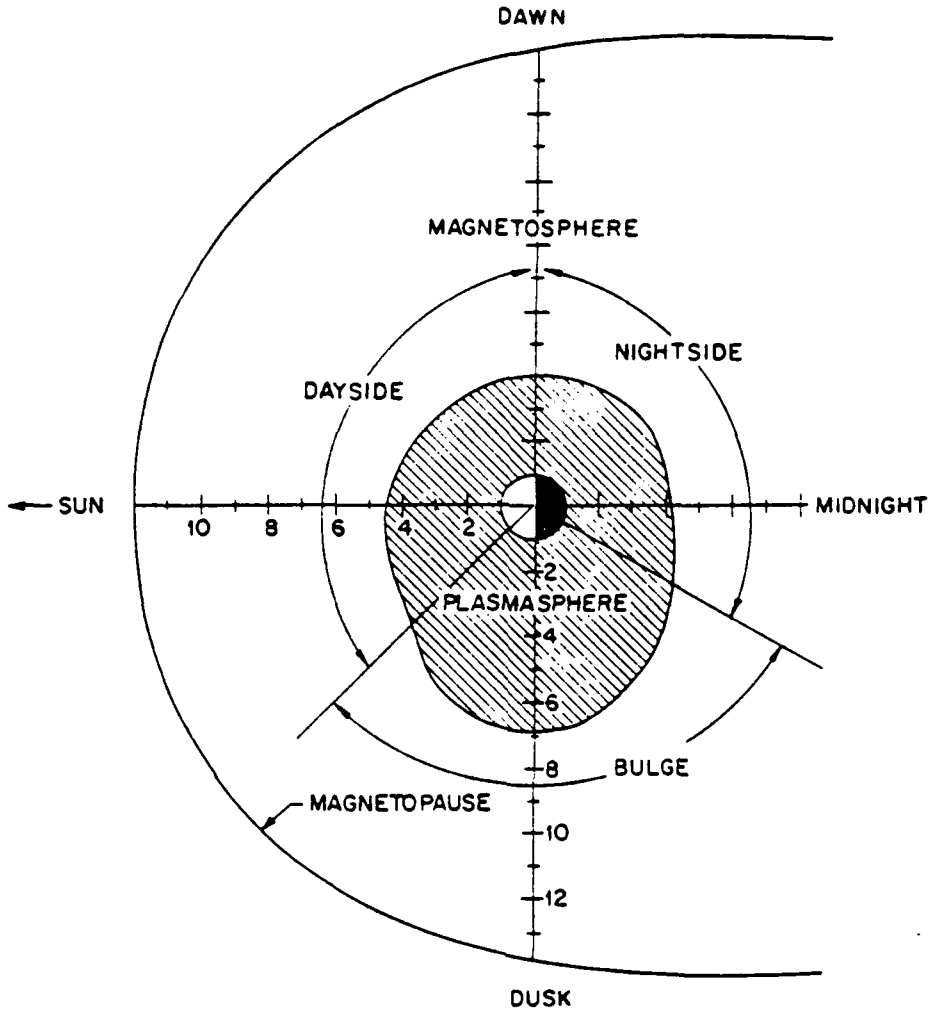

Figure 2. The average position of the plasmapause shown in the equatorial plane (Chappell, 1979).

II. THE SCATHA PROGRAM

A. SATELLITE DESCRIPTION

The Air Force P78-2 SCATHA (Spacecraft Charging AT High Altitude) satellite, part of a joint program with NASA, was designed to study the causes and dynamics of spacecraft charging. It was launched January 30, 1979, and reached its final near geosynchronous orbit on February 2, 1979. The satellite is cylindrical in shape, approximately 1.7 m in length and 1 .75 m diameter, and has seven experimental booms. It is spin stabilized and rotates with a period of 59 seconds about an axis which lies in the orbital plane and is nominally perpendicular to the earth-sun line. The orbit is elliptical, with perigee of 5.3 R_E, apogee of 7.8 R_E, and period of 23.5 hours. The orbital plane was inclined 7.8° and the satellite drifts eastward about 5.1° a day. The satellite is eclipsed for about one hour periods every day for 40 days around the spring and fall equinoxes.

Many of the instruments are contained around the middle of the cylinder in an area called the belly band, which contains both insulating and conducting materials. The "top" of the satellite is a conducting surface and the "bottom" is composed of insulators. Solar cells make up most of the remaining parts of the cylinder. Figure 3 shows the location

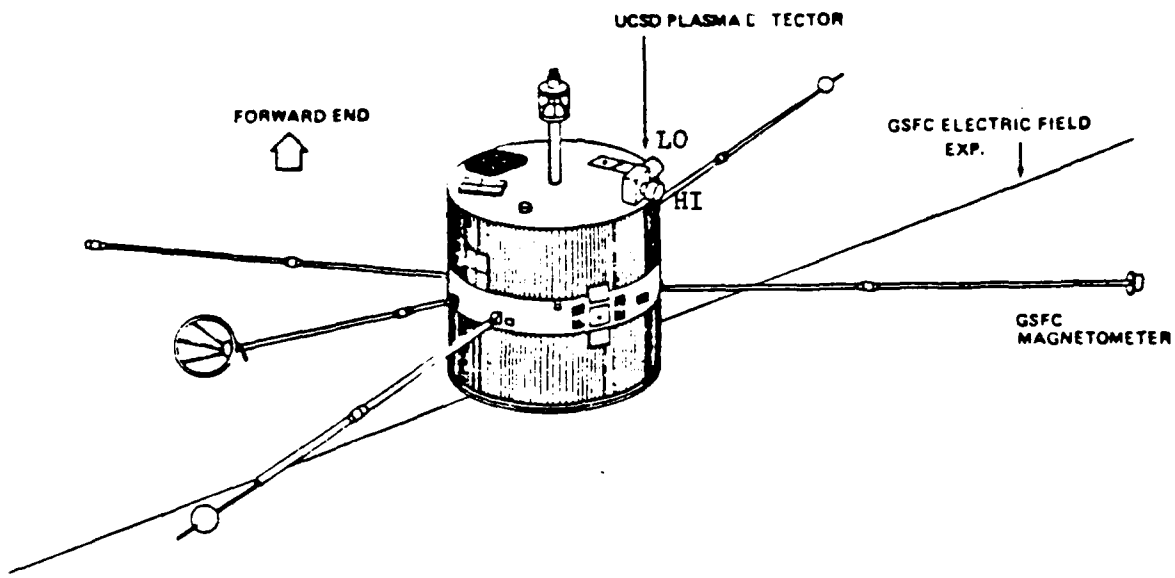

Figure 3. The P78-2 SCATHA satellite.

of several of the experiments on the satellite. The P78-2 experiments used for this work are the ion gun, the plasma detectors, and the electric field monitor. (Fennel, 1982)

B. UCSD PLASMA DETECTORS

The University of California at San Diego charged particle experiment (SC9) consist of five electrostatic analyzers, three for ions and two for electrons. Pairs of ion and electron ESA's are mounted on the top of the satellite in rotating heads which sweep in orthogonal planes over a 220° range through the spin axis and radially outwards. The detector geometry and rotation angles are shown in Figure 4. The third ion detector is mounted to look radially outward. One of the rotating assemblies (the HI or NS detector) has an energy range of 1 eV to 81 KeV. The other rotating assembly (the LO or EW detector) and the single ion detector (FIX detector) have an energy range of 1 eV to 1800 eV. Energy resolution is 20% with adjacent channels overlapping in coverage. The angular field of view is 5 X 7 degrees. The outputs of the rotating detectors are sampled 4 times a second and the fixed detector is sampled at 8 times a second. Pitch angle distributions are obtained by parking the detectors so that they look perpendicular to the spin axis.

Using particle detectors to determine vehicle charging has drawbacks. They are not positioned on the satellite

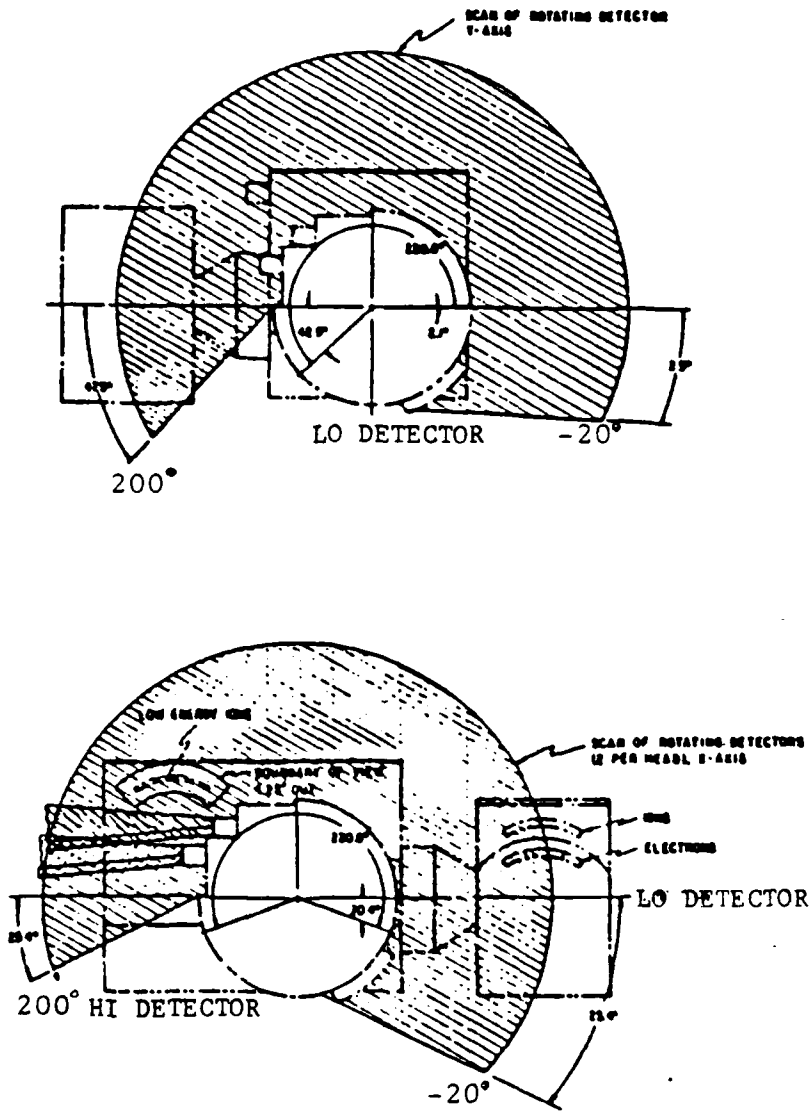

Figure 4. Charged particle detector (SC9) geometry.

with detection of charging as their prime objective. Energy channel widths and sampling intervals are therefore not optimal. Also, the ambient ion flux is sometimes magnetic field aligned and if the detector is not looking in the right direction or energy range, a charging peak will not be observed. (Fennel, 1982; SCATHA Handbook, 1980)

C. ELECTRIC FIELD MONITOR

The NASA Goddard Space Flight Center electric field monitor experiment (SC10) experiment consists of dipole antennas (cylindrical double floating probes) 100 m tip-to-tip in length and projecting into the spin plane. One of the uses of the experiment was to measure the satellite potential relative to the sensor's during spacecraft charging events (Aggson et al., 1983). The antennae are beryllium copper tubbing insulated except for the last 20 m with a kapton coating, providing an 80 m baseline. The booms are electrically isolated from the satellite body.

A schematic of the two different modes of this experiment is shown in Figure 5. The ambient electric field is obtained from differential signals between the antennas (the differential mode). The data used in this paper is from the common mode, which measures the voltage of one antenna relative to the spacecraft ground with a time resolution of 0.5 seconds.

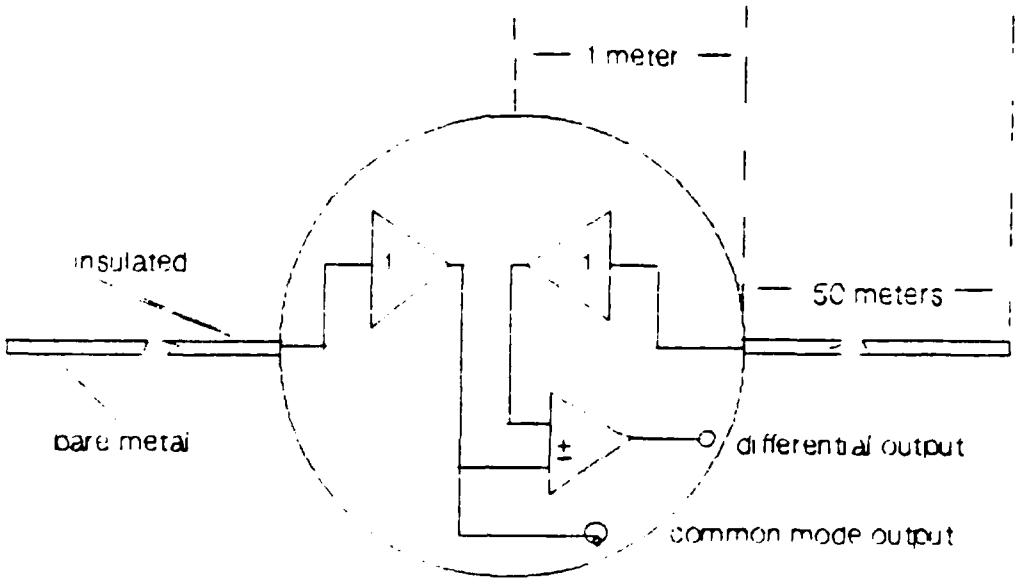

Figure 5. Schematic showing SC10 common and differential mode outputs.

It has been shown that the SC10 experiment measures spacecraft potential very accurately in sunlight (Mullen et al., 1986). This is because copper beryllium, which constitutes the outer 20 meters of the boom, has such a high secondary electron coefficient (meaning abundance of secondary emission) that significant negative charging does not occur in most plasma environments (Lai et al., 1986). Hence, the antennae can be considered, to a reasonable approximation, to be at independent floating potentials.

Graphs of the SC10 data shows that the vehicle potential changes very rapidly with sun angle. During the periods when the antenna points directly at the sun or is in the shadow of the satellite, the antenna also charges somewhat due to the absence of photoemission. The measurement then actually represents the potential difference between the charged boom and the charged vehicle and not between the charged vehicle and the ambient plasma (Lai et al., 1986). The charging of the antennae becomes important during periods in which the spacecraft is not charged to high voltages. Part of this paper will address the interaction of ion beam ejection, photoemission, and satellite charging.

D. ION GUN

The Satellite Positive-Ion-Beam System (SPIBS) is the AFGL ion gun experiment (SC4-2) developed by Hughes Research

Laboratories. It is located on the bottom of the satellite and is used to emit electrons, beams of positive ions, or beams containing both. The SPIBS instrument was designed to create several different spacecraft ground-to-ambient plasma potential differences and to investigate various techniques for maintaining spacecraft ground at or near the potential of the ambient plasma.

The basic system consist of a power supply, an ion source, and an expellant assembly. Positive Xenon ions are accelerated electrostatically to a high velocity. The discharge is operated at the beam potential to allow the ions to exit at near ground potential. Ions are formed in the discharge plasma by collisions between atoms and electrons. Electrons are generated using a conventional hollow cathode. The electrons are then accelerated into the plasma by means of the discharge voltage. An axial magnetic field restricts electron flow radially and increases electron-atom collisions. A neutralizer (thermionically emitting filament) is located downstream of the ion accelerating structure. The neutralizer can be used to neutralize all or a fraction of the beam and can be biased to $\pm$1000 V to control satellite potential relative to the plasma. The neutralizer and the ion source can be operated independently. Figure 6 is a block diagram of the ion gun

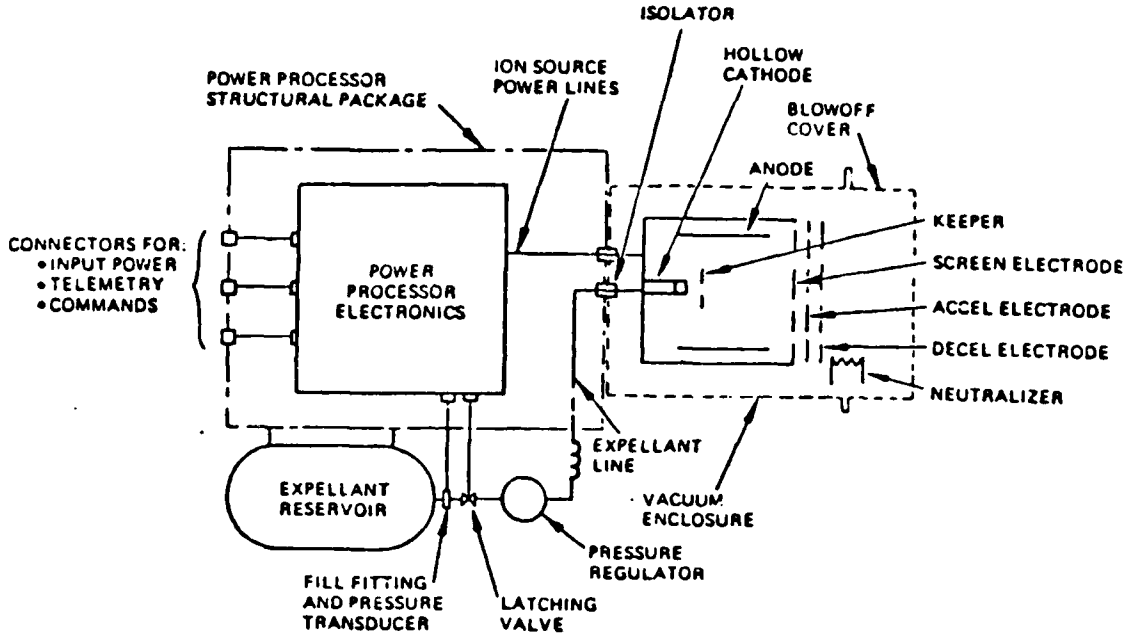

Figure 6 . SC4-2 ion gun block diagram.

system and Figure 7 is an electrical schematic indicating the general electrical interconnections.

Unneutralized ion beam current levels can be set from 0.3 mA to 2 mA at energies of 1 and 2 KeV. In addition to the normal operating modes, there is a "trickle mode" which occurs when the beam voltage is switched off and the keeper remains on. The keeper is the means for starting and maintaing the discharge and all Xenon flows through the cathode and the keeper. In trickle mode, the beam discharged is 20 - 80 microamps and of low (essentially thermal, ~1 eV) energy.

The beam current is measured in several ways. The beam current telemetry value is the current passing through the beam power supply. The net beam current is the measured beam supply current reduced by the sum of the accel and decel currents. Therefore, the SPIBS net current, measured at spacecraft common as shown in the schematic of Figure 8, more accurately defines the current leaving the ion gun. The SPIBS net current is measured by a bipolar electrometer, whose output is accurate to $\pm$10% of the true current (for positive or negative currents greater than 2 microamps). Neutralizer emission and net currents (ion and electron) between the SPIBS instrument and the satellite ground can be detected down to a level of 2 microamps. (Masek and Cohen, 1978; Masek, 1978))

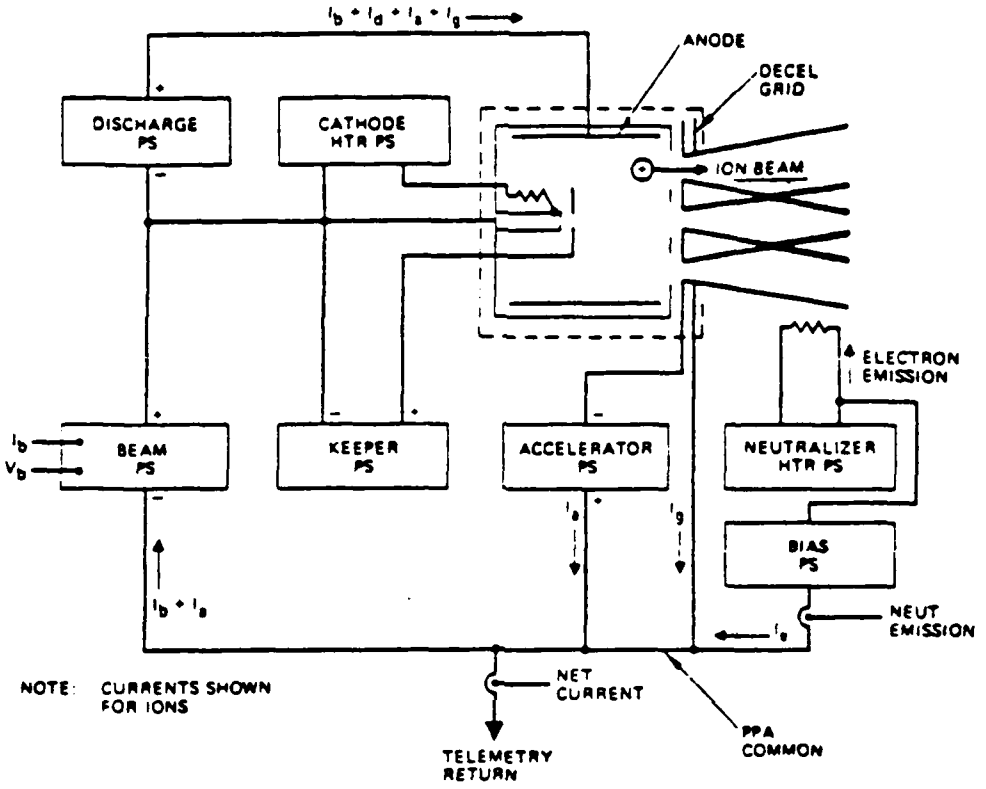

Figure 7. SC4-2 ion gun electrical schematic.

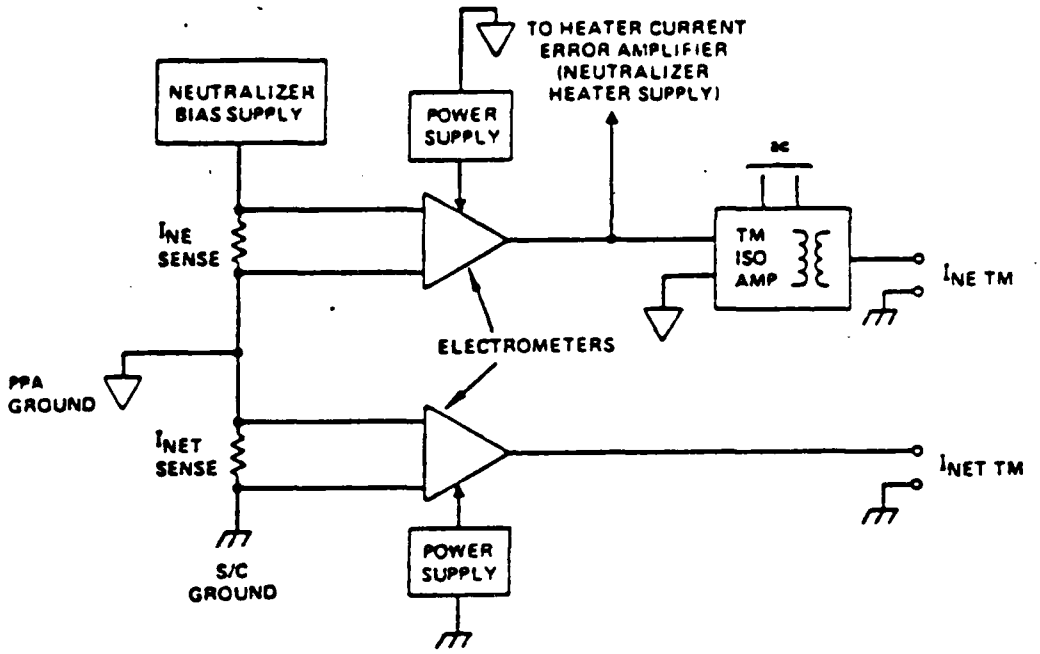

Figure 8. Electrometer block diagram.

III. OBSERVATIONS

In this thesis, results from four sets of observations will be presented. Data from the UCSD particle detectors (SC9) and the GSFC electric field monitor experiment (SC10) will be used to investigate the effects of emitting an ion beam from a spacecraft in geosynchronous orbit. The observation days to be presented were chosen to demonstrate various modes of ion gun operation in both sunlight and eclipse.

The first set of observations concern the satellite in sunlight. The ion gun is operated in a high energy, high current mode which induces a large negative potential. Also discussed is a low energy, low current mode termed "trickle mode"[1]. The SC10 experiment is examined to determine if it accurately measures spacecraft potential during sunlight ion emission. The second set presents ion gun operations in a different environment and builds on work already reported by Olsen (Olsen, 1987). The gun is operated in sunlight at a

---

[1]NASA's Polar satellite, part of the NASA Global Geospace Science (GGS) program, is planned to have a hollow cathode source which will produce an ion flux equivalent to trickle mode. It is due to be launched in 1992.

slighty lower current. A 1 kV, low current mode[2] is also examined here. This section concludes with two similar sets of observations of the spacecraft in eclipse. Here the spacecraft's response to different beam voltages and currents is examined and compared to sunlight operations. The SC10 potential measurement is also validated for eclipse. Lastly, the satellite's capacitive response to termination of ion emission is discussed.

A. DAY 200

Data from operations on 19 July, 1979 (Day 200), are presented first to illustrate two modes of operation of the ion gun in sunlight. The first example of ion emission begins shortly after 2140 UT. The satellite located in the plasmasheet near local dusk (1954-2042 LT) between L = 7.6 and 8.0, at an altitude of 7.5 R_E and a magnetic latitude of 6 degrees.

The particle data for this day are summarized in spectrogram format in Figure 9. In a spectrogram, instrument count rate (or particle flux) is plotted as a function of time on the horizontal axis and energy on the vertical axis.

---

[2]Low current mode is applicable to the European Space Agency Cluster satellite liquid metal ion gun. This is a 10 - 20 microamp, 7 kV device to be flown in 1995.

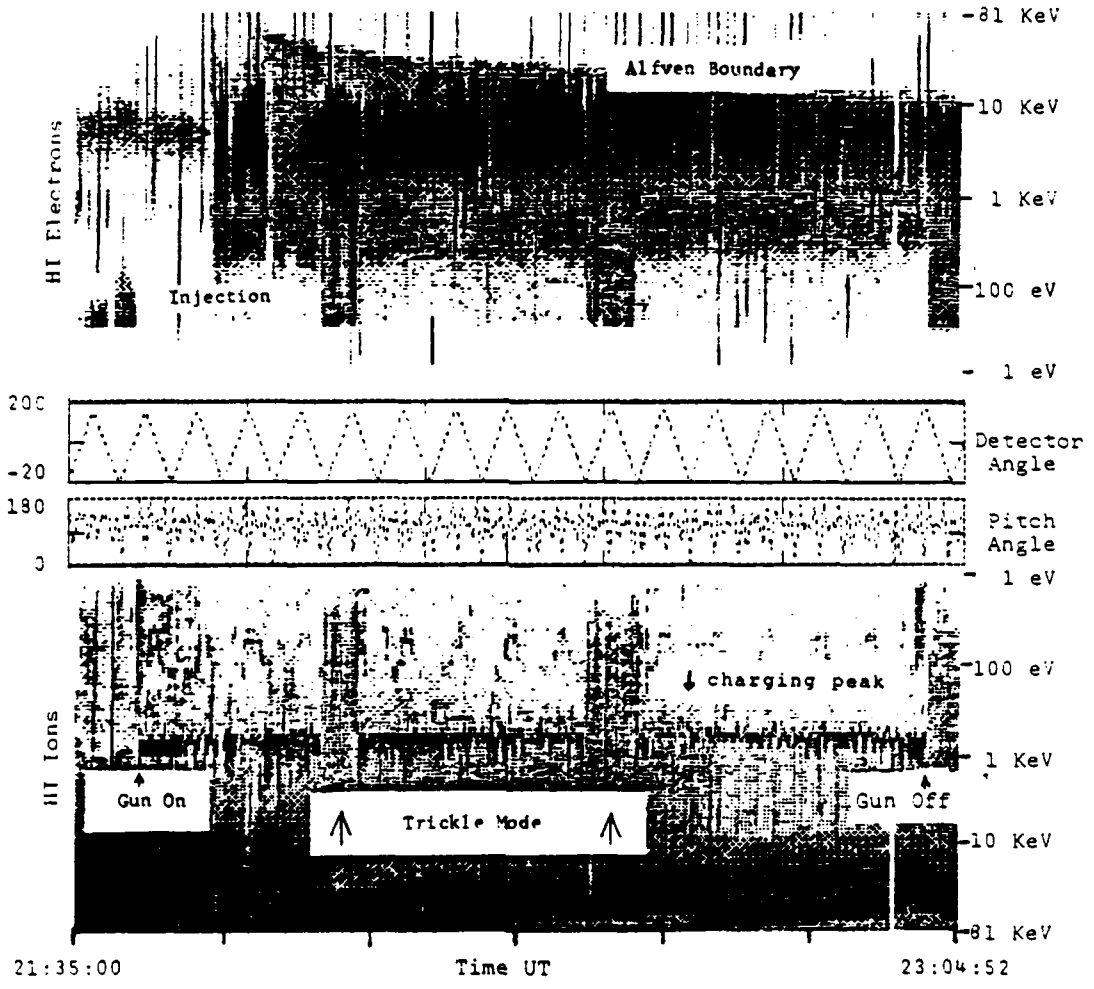

Figure 9. Spectrogram for ions and electrons, Day 200 of 1979.

The flux magnitude is depicted using a gray scale, with high fluxes appearing as dark gray or black and low or zero fluxes showing up as light gray to white. This figure displays data from the two high-energy detectors, with the electron data on top. The energy axis is zero in the middle of the figure and increases upwards for the electrons and downwards for the ions. The lower horizontal line plot in the center is the pitch angle of the measured particles. The pitch angle is the angle between the particle's velocity vector and the magnetic field line. The upper horizontal line plot is the detector head angle (see Figure 4). Note the plasma injection at 2149 UT, recognized by the abrupt increase in particle flux over a wide energy range. Injections are the sudden appearance of hot plasma and occur at least daily, more frequently during periods of high magnetic activity, with variable spectra (McIlwain and Whipple, 1986). The peak in the differential electron flux (count rate) is in the 1 to 10 KeV range, typical for the plasma sheet. The upper bound on the electron flux (~10 KeV) is the result of magnetospheric convection processes and is termed the Alfven boundary. It must exceed a critical energy of 15 to 20 KeV for negative charging to occur. The high energy ion flux extends up to 80 KeV.

Unneutralized ion gun operation at 1 kV and a current setting of 1 mA begins at 2141 UT and terminates at 2301 UT.

This results in satellite charging, as seen in the ion spectrogram as a black band representing high ion fluxes. The high fluxes are due to ambient low energy ions being accelerated into the spacecraft at the spacecraft potential energy. There are two periods of trickle mode operation (no accel voltage), 2200-2203 UT and 2227-2232 UT, which correspond to the times in the spectrogram where the black ion flux band is absent. This suggests a spacecraft potential magnitude of less than 10 Volts.

Electron and ion data for the 0-80 KeV energy range, taken from the HI detectors at 22:01:56 UT, are presented as distribution functions in Figure 10, in order to characterize the environment. The distribution function, or phase space density, is proportional to the count rate divided by the square of the energy. In this format, a Maxwellian distribution would appear as a straight line. The density and temperature of the observed particles, calculated from the distribution functions using a piece-wise least squares fit method, is given in Table II. Density and energy can also be obtained by taking the moments of the distribution function. This is also shown in Table II. The density estimate obtained by integrating the distribution function can have several flaws.

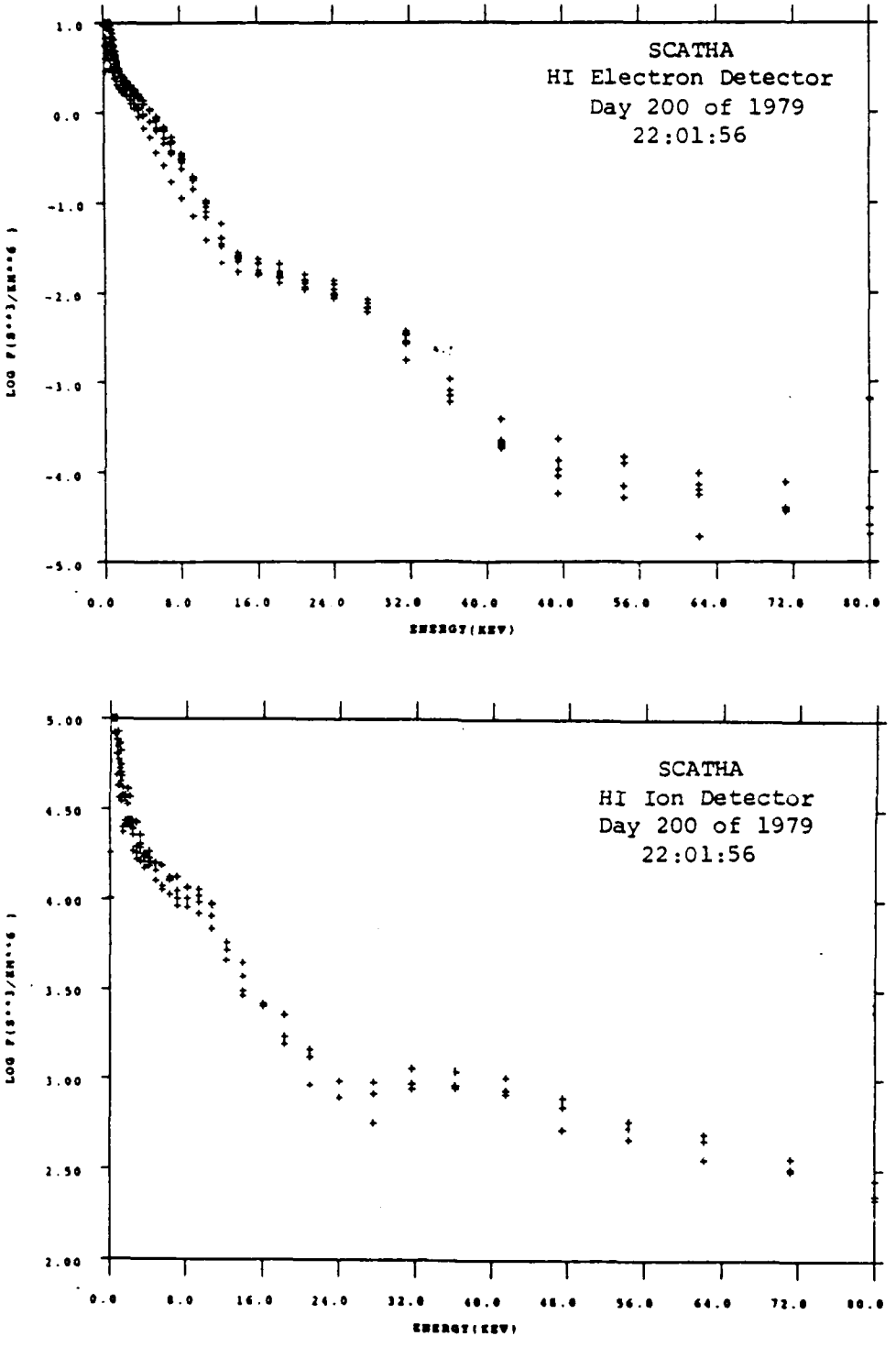

Figure 10. Electron and ion distribution functions, Day 200.

For ions:

a) a positive satellite potential will repel low energy ambient ions, resulting in an underestimate of density.

b) pitch angle distributions are typically anisotropic, but the assumption of isotropicity is made. Most of the measurements are biased towards perpendicular ions.

c) the mass assumption made in calculating the distribution function from the count rate is that m = 1 amu (proton). This results in an underestimate of density by up to a factor of 4 if the ions are O^+. Typically, O^+ is about 20-50% of the ions, so the density is underestimated by a factor of 2.

For electrons:

a) a positive satellite potential results in trapping locally generated photoelectrons. The integration stopped to avoid this contribution, but density can still be overestimated. Note that $\exp(e\Phi/kT)$ is greater than one for electrons for a positive satellite.

TABLE II

DAY 200 PIECE-WISE MAXWELLIAN PARAMETERS

	Energy Range	Density (cm-3)	Temperature
Electrons:	100-1200 eV	0.69	306 eV
	4 - 10 KeV	1.15	2.6 Kev
	10 - 80 KeV	0.13	8.3 KeV
Moments:	50 eV-80 KeV	1.43	2.2 KeV
Ions:	10 -500 eV	0.17	139 eV
	1 - 25 KeV	0.008	14.1 KeV
	20 - 80 KeV	0.0028	167 KeV
Moments:	1 eV-80 KeV	1.34	3.6 KeV

Trickle mode operation will be examined first and some of the results applied to the observations of 1 kV ion gun operation.

1. Low Energy, Low Current Mode

a. Observations

Figure 11 is an example of the SC10 potential in trickle mode operation. In trickle mode the beam voltage is switched off and the keeper remains on, allowing the ions to diffuse out of the gun. Two spin periods are shown with the ion gun current, taken from the SPIBS net current monitor telemetry, plotted on the bottom of the figure. The SC10 data indicates the mainframe is within a few volts of the antenna potential, and hence near plasma potential. Both the probe voltages and the net ion gun current are modulated, and by inference, so is the spacecraft mainframe potential. This may be explained by examining the effect of solar radiation on the satellite.

b. Analysis

Since the photocurrent is the major current from the spacecraft at geosynchronous orbit, the surface material properties greatly influence the spacecraft ground potential. Especially important are the conducting surfaces grounded to the spacecraft frame. The normal to the top and bottom of the satellite are close to perpendicular to the sun and thus their materials do not contribute significantly

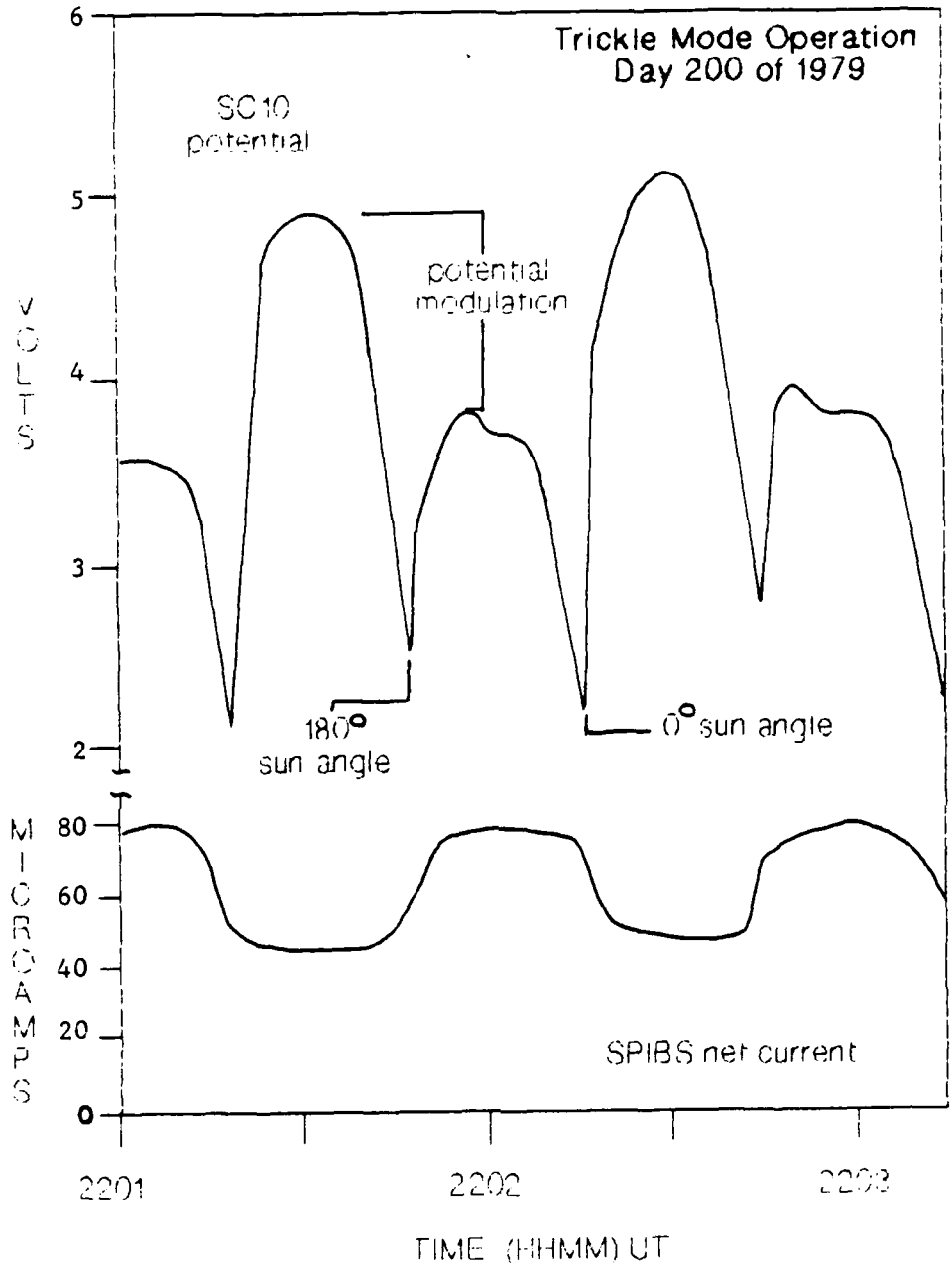

Figure 11. SC10 and SPIBS net current during trickle mode.

to the photocurrent. Most of the conducting material is contained in the band around the middle of the cylinder that contains the instruments. There is also a significant area of indium oxide coating, a conductor, on the solar cells under the SC9 instrument.

The total photocurrent of illuminated exterior grounded conducting surfaces from the SCATHA satellite at 0 Volt potential has been calculated by Craven (Craven et al., 1987) as a function of the rotation angle from the sun. The calculated photocurrent varies from 8 to 20 microamps and is shown in Figure 12. This figure also shows the relationship between this total photocurrent, the ion gun net current, and the SC10 potential as a function of the angle between the SC10-2 boom and the sun. This illustrates how the small potential modulations are strongly linked to the material properties of the conducting surface areas grounded directly to the spacecraft frame and can be understood by considering the balance of currents to the spacecraft.

In the steady state, satellite potential is governed by the balance of incoming and outgoing current:

$$I_r - I_e = I_b - I_{ph}$$

where I_e is the ambient electron current (less secondaries), I_{ph} is the photoelectron current from the spacecraft, I_b is the ion beam current, and I_r is the returned beam current.

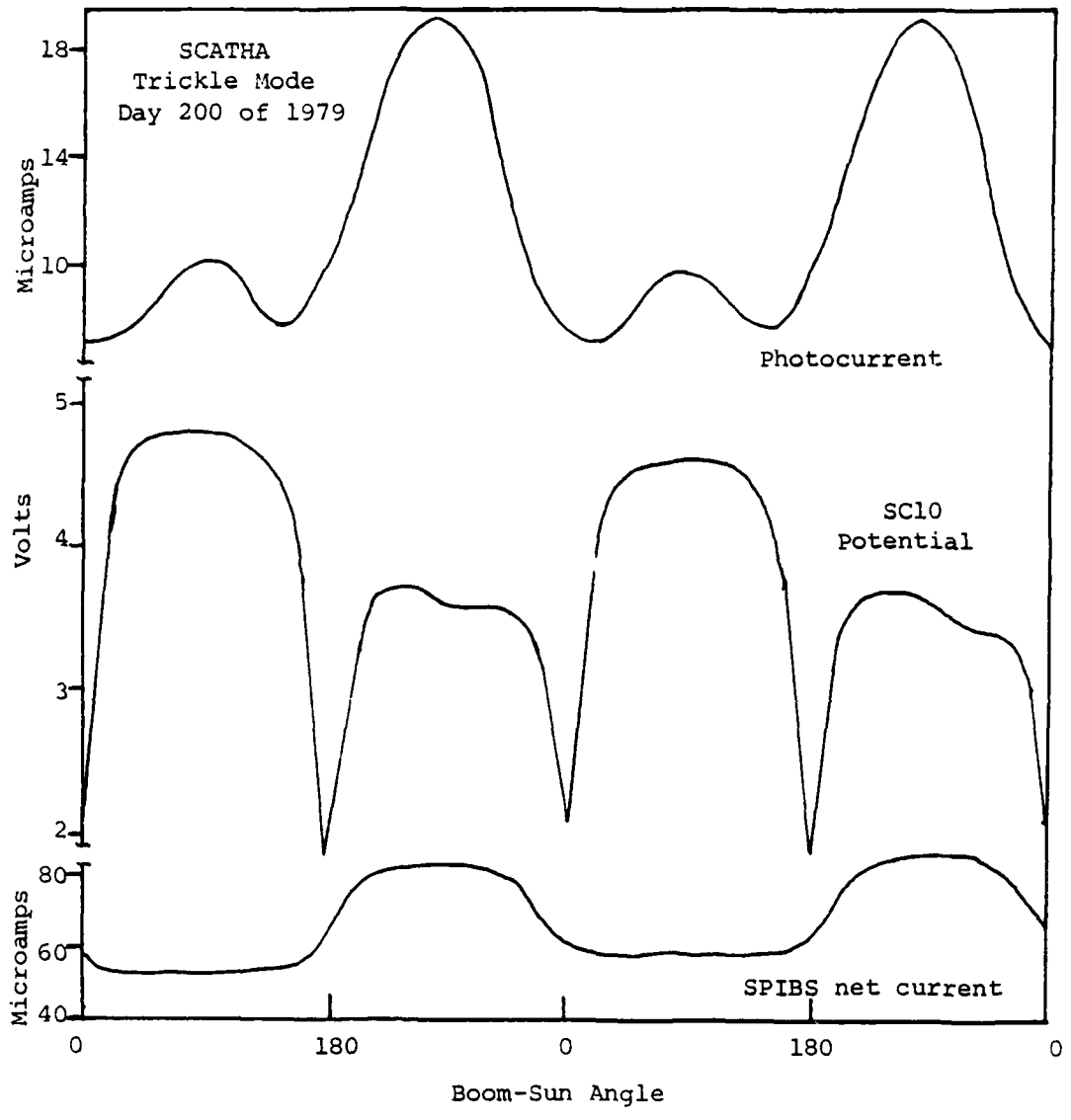

Figure 12. Photocurrent, ion gun net current, and SC10 potential as a function of boom-sun angle.

One additional term that can be significant is the photocurrent between the booms and the spacecraft. For a small positive potential on the satellite, the effect of the photoelectrons from the booms is negligble (Lai et al., 1987). Conversely, for a small negative potential on the spacecraft, the fraction of the photoelectron current going to the booms is negligible. The ambient ion currents are usually much smaller than the ambient electron currents and may be ignored. The ambient electron currents (less secondary emission) are generally important in charging, but for Day 200 in sunlight are small enough relative to the others to neglect. If the spacecraft potential is positive, as in this case, the return current I_- can be disregarded. For potentials less than the beam energy the return current is negligible because all the ions from the source should escape (unless scattered for some reason). Hence, the major terms are the photocurrent and the ion source current. The satellite potential (and hence the SC10 measurement) is the result of the balance between these two. In trickle mode, the net emitted ion current is determined by the spacecraft potential and is probably proportional to $\exp[e\Phi/kT]$.

Using the SC10 data, first order values for the spacecraft potential in trickle mode and with the ion gun off can easily be found. The expected behavior of the common mode voltage, as derived from probe theory during periods

of no appreciable charging, varies as the satellite rotates in angle (Ø) like ln(sin Ø). The oscillatory variations at twice the satellite spin period are due to changes in probe illumination. The negative spikes every half spin period are due to the singularity in the ln(sinØ) dependence of the boom potential. Physically, the singularities are due to the suppression of the photocurrent when the antennae are at grazing angles relative to the sun vector. When the antennae are directed along the sun-satellite line, they are at their minimum or most negative potential with respect to the satellite. At this point, the antennae are closest to plasma potential. At or near normal sun angles, the boom is close to its maximum potential. The one volt modulation of the maxima is caused by a change in the spacecraft ground due to the various exposed conducting surfaces directly grounded to the spacecraft frame and not from a difference in the illumination of the antennae (Craven et al., 1987).

An approximate value of 5.4 Volts for the maximum SC10 boom potential was determined by Lai (Lai et al., 1986). Using this value for the maximum boom potential, the theoretical boom potential is plotted in Figure 13, along with the measured SC10 potential for ion gun off and trickle mode operation, as a function of sun angle. The approximate magnitude and variation in spacecraft frame potential can be obtained by taking the algebraic difference

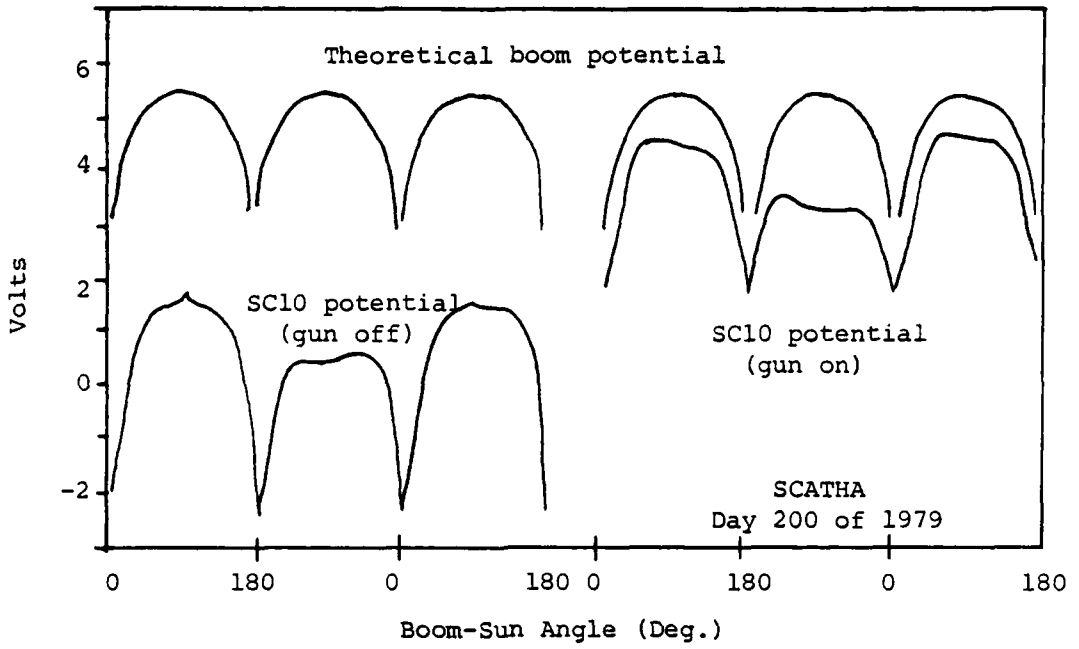

Figure 13. SC10 potentials for ion gun on and off.

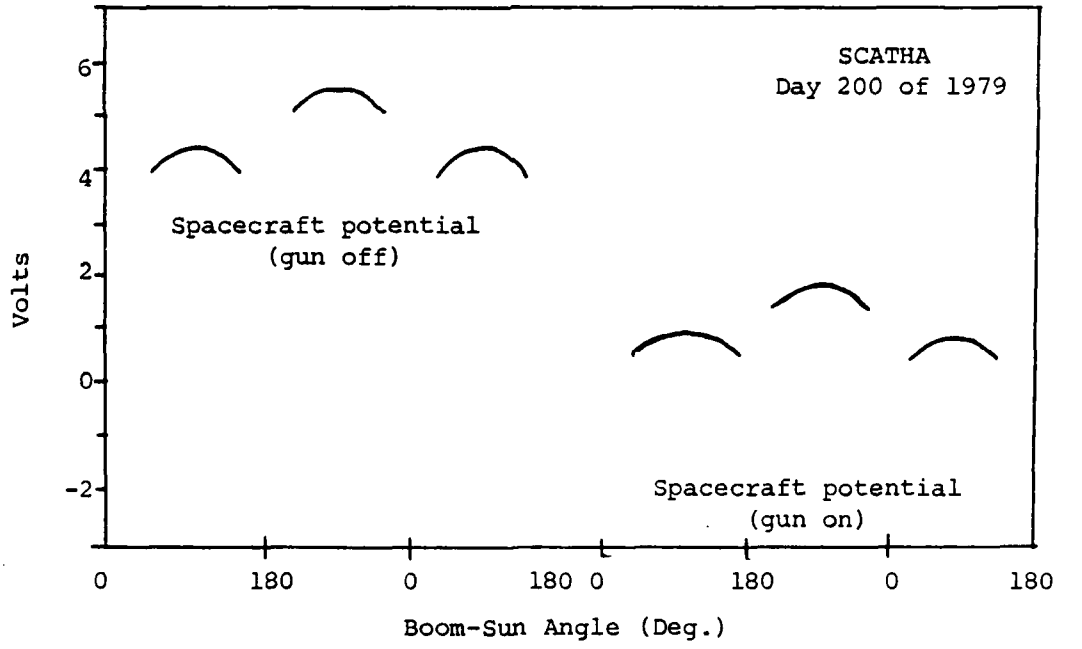

Figure 14. Estimated spacecraft potentials for ion gun on and off.

between the boom potential and the SC10 measured potential and is shown in Figure 14. The gaps represent the periods when the antenna was pointing directly at the sun or in the shadow of the satellite. The ion gun had no effect on the 1 Volt potential modulation but reduced the spacecraft frame potential to just slightly positive.

The distribution of the emitted photoelectrons is approximately an isotropic Maxwellian with a most probable energy on the order of 1.5 eV (Grard et al., 1983). Since a spacecraft potential of about +5 volts will effectively shut off the photocurrent, a potential just slightly positive is consistent with the requirement that most of the photoelectrons escape in order to cause the observed potential modulation.

Because the injected ions and the photoelectrons are of low energy, the currents are modulated as $\exp[e\xi/kT]$. Since $T \sim 1$ eV and $\xi \sim 1$ Volt, $\exp[e\xi/kT]$ has a value near 2. This agrees with the modulation from 40 to 80 microamps seen in the net current. There is however, a disparity in the magnitudes of the photocurrent and the ion current, since the two should be roughly equal. Thus it appears that either the calculated photocurrent (laboratory values vary considerably in their estimations of photoyield values) or the SPIBS calibration is off by a factor of 2 to 4. It

should also be noted that this does not affect the validity of Craven's results.

2. High Voltage, High Current Mode

When the ion gun is activated at 2141 UT, the satellite is driven to a potential between 600 and 800 volts negative, which is significantly less than the beam energy. This is indicated in the spectrogram by a black band representing high ion fluxes. The ion flux peak is due to the ambient low energy ions being accelerated into the spacecraft at the spacecraft potential energy. Potentials of less than about $\pm$10 Volts are difficult to determine using this method, as seen by the complete absence of any ion charging peak during the two trickle mode operations. The spacecraft potential is most accurately determined by converting flux (count rate) to the particle distribution functions. The peak at about 700 eV in the ion distribution function of Figure 15, taken at 22:10:44 UT, is interpreted to be at the spacecraft potential. Representative energy channel widths are shown using bars on the data points. Note that the energy channels overlap.

Figure 16 is a plot of the potential as measured by the SC10 experiment. A minimum of two points (the high and low values) are plotted per spin period. A modulation at the spin period is immediately obvious. There is a turn on transient, also seen in the SC9 data (not shown), indicating

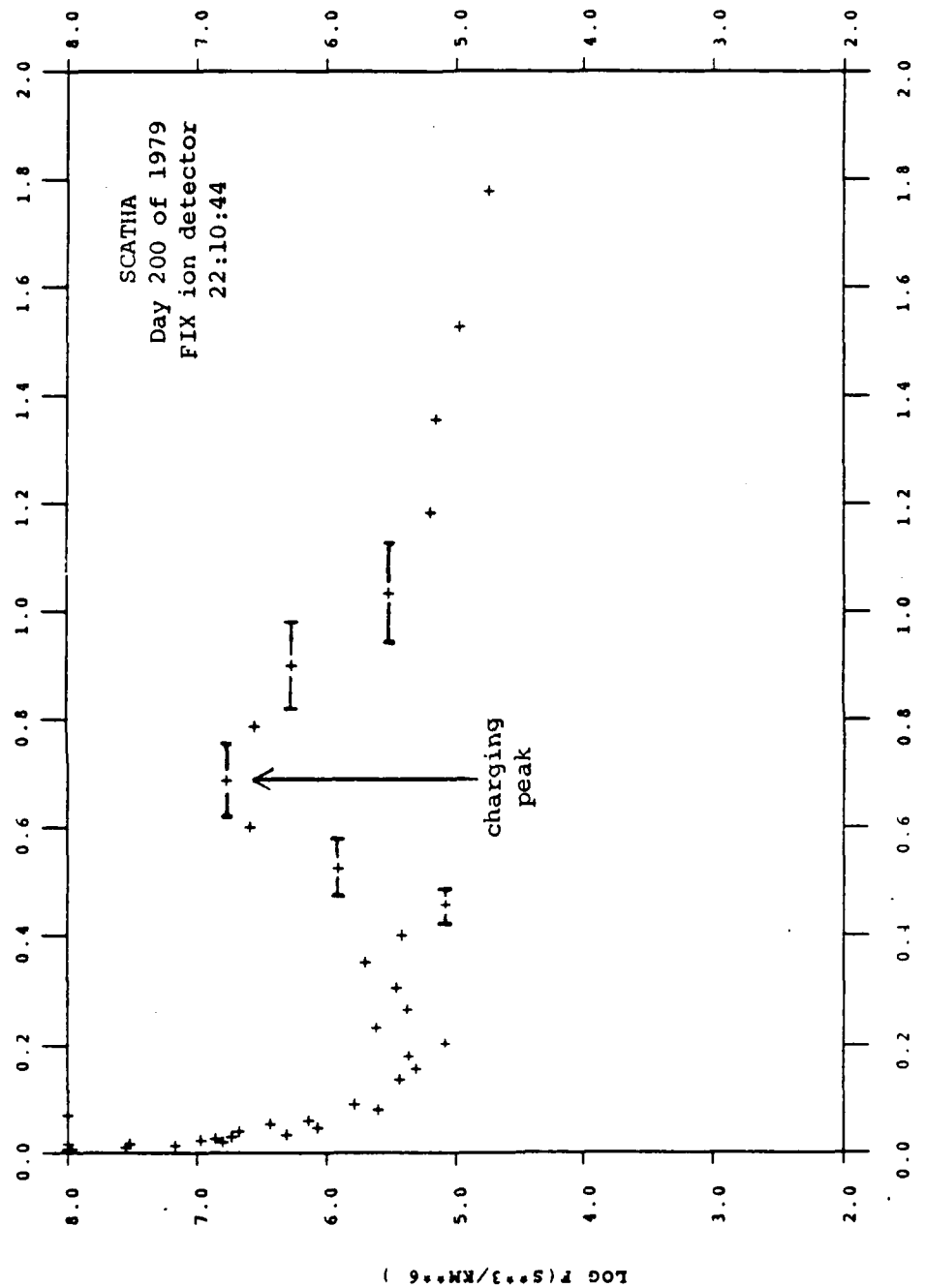

Figure 15. Ion distribution function, Day 200 of 1979.

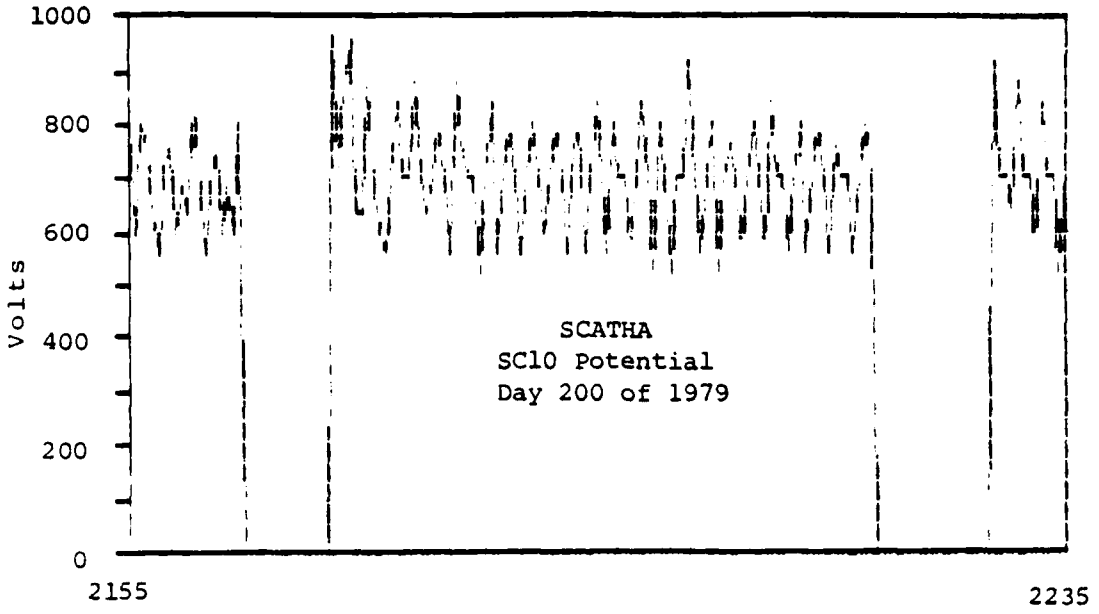

Figure 16. SC10 potential, Day 200.

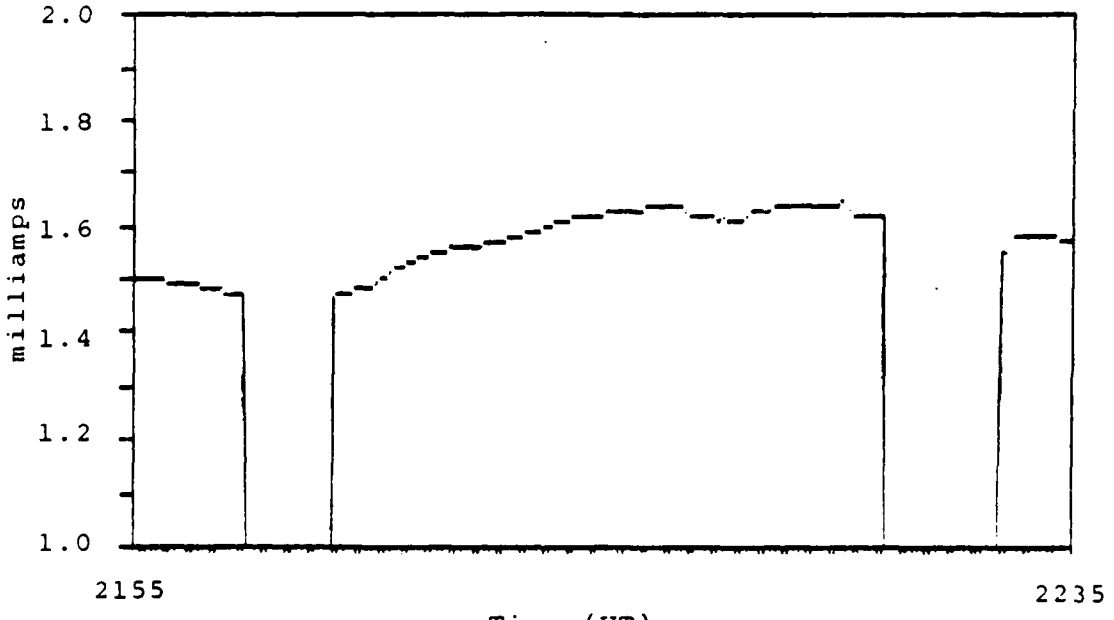

Figure 17. Ion gun beam current.

the spacecraft momentarily charges to a negative potential corresponding to the magnitude of the beam voltage. The spacecraft potential then rises (becomes less negative). This behavior is seen each time the gun is switched on and is counter-intuitive as the beam current, plotted in Figure 17, actually increases during the transient. Note that the beam current is measured at the beam power supply and the net beam current, which stays constant, is measured at spacecraft common.

Figure 18 shows greater resolution for a period after the turn on transient and is representative of normal ion gun operations for Day 200. It shows the potential, with points plotted every two seconds, as measured by SC10 between 2210 UT and 2215 UT or for approximately five spin periods. Also plotted in this figure is the spacecraft potential as determined by SC9 charging peaks for the HI and LO detectors. Energy channel widths are shown for representative SC9 data points. The excellent agreement between the SC9 and SC10 values suggest that the SC10 experiment provides a valid measurement of the spacecraft potential during ion-emission induced charging events in sunlight. The resolution of the SC10 experiment is 40 V for measurements above 300 V. This and the difficulty in picking the channel of the ion peak may account for some of the small differences between SC9 and SC10 values.

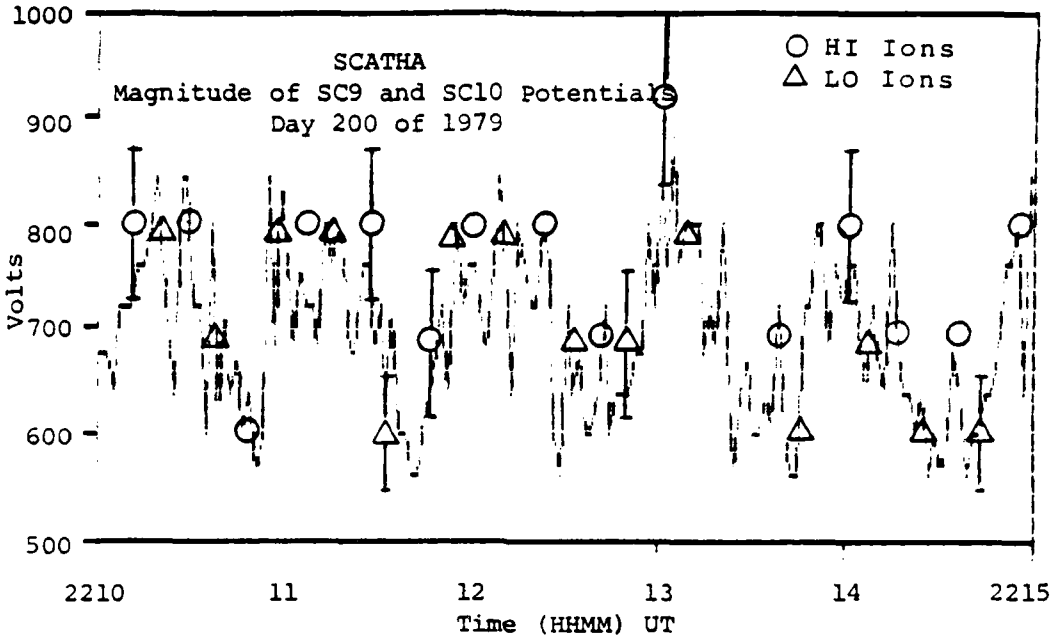

Figure 18. SC9 and SC10 potentials, Day 200.

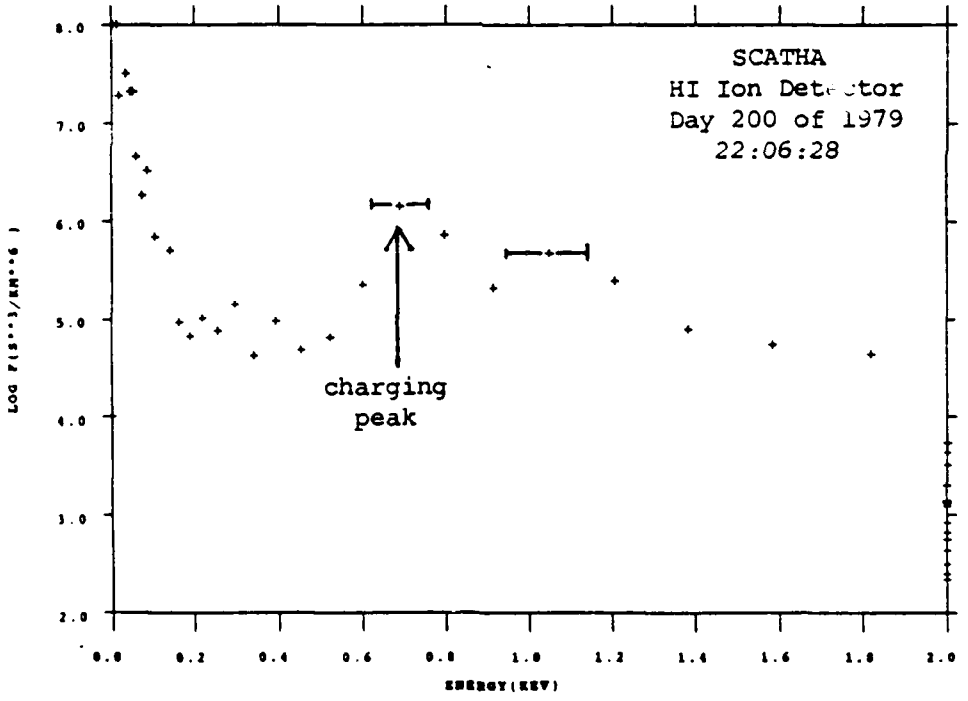

Figure 19. Ion distribution function, Day 200.

Normal operation of the ion gun for this observation period is characterized in the SC10 data by large, rapid noise-like fluctuations, not present during gun off or trickle mode operations, and the previously mentioned spin modulation peaking once per minute. The SC9 data appear to confirm that the spacecraft frame potential is indeed rapidly fluctuating. The SPIBS Net Beam Current telemetry is constant during this period. Since the electrometer outputs are accurate to $\pm$10% of the true current, gross variations in the beam caused by sputtering or other mechanisms within the ion gun do not appear to be the cause. Given the failure of the satellite to charge to the beam energy, it seamed reasonable to search for signs of the beam in the 1 kV channel.

Figure 19 shows a distribution function taken during ion gun operation at 22:06:28 UT. Representative energy channel widths are shown using bars. The significant feature of this figure is the second peak at an energy greater than the spacecraft potential and near the ion gun energy. This secondary peak appears to be the 1 KeV beam ions scattered into the UCSD detector. Figure 20 shows a portion of the ion distribution function for ten energy sweeps taken over a three minute period. Of note is the variation of the distribution function around the 1 KeV energy channel. The detector angle and pitch angle are given for each 1 KeV

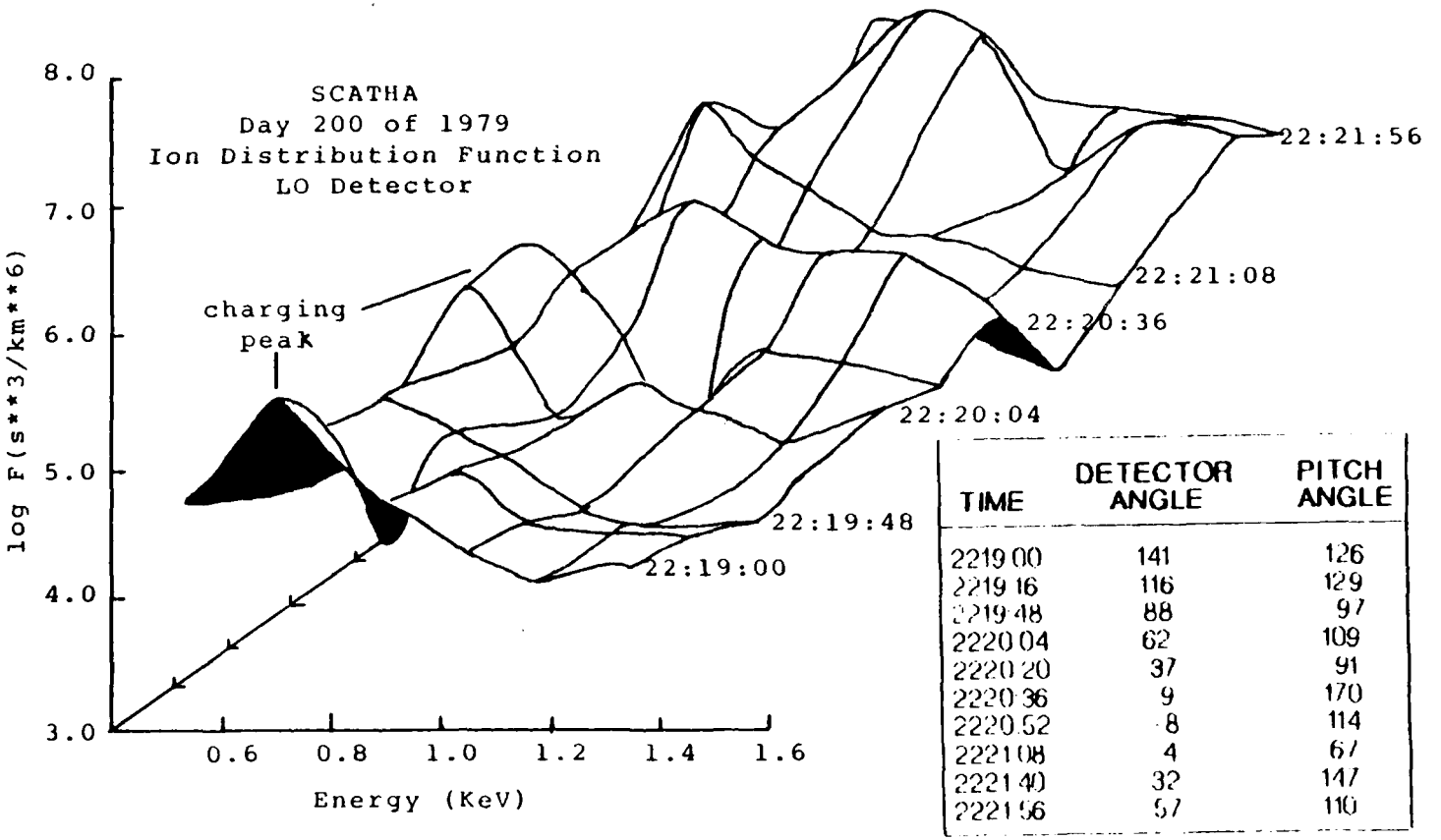

TIME	DETECTOR ANGLE	PITCH ANGLE
221900	141	126
221916	116	129
221948	88	97
222004	62	109
222020	37	91
222036	9	170
222052	8	114
222108	4	67
222140	32	147
222156	57	110

Figure 20. Time variation of ion distribution function, Day 200.

sample. The satellite potential is -0.7 to -0.9 kV with a strong secondary peak at 1 kV most evident at 2220 UT. No statistical analysis or correlation of the second higher energy peak to the detector head angle or the particle pitch angle was attempted. This type of temporal behavior in the distribution function is typical of Day 200 ion gun operation (excluding trickle mode). It may indicate that periodically, significant fluxes of ions at or near beam energy are being returned to the satellite.

The potential modulation seen in Figures 16 and 18 peaks once per spin period. This indicates the boom sun angle is not a significant factor since this would introduce two peaks per spin period as seen in the case of electron beam injections. During electron beam injections the two peaks per spin period are due to boom-generated photoelectron currents flowing toward the satellite (Lai et al., 1987). The spin modulation seen during ion gun operations is not observed in eclipse (see Day 293 and Day 295 observations), suggesting the sun is the driving influence. To investigate further, the orientation of the satellite relative to the sun was determined.

The singularities observed in trickle mode occur at a boom-sun angle of 0° and 180°. By examining the SC10 data around the ion gun transition from full on into trickle mode, the phasing of the spin modulation can be determined.

As seen in Figure 21, which depicts the 2200 UT transition into trickle mode, the minima occur at a boom sun angle of about 300°. The second transition into trickle mode at 2227 UT yielded the same result. Thus the satellite's orientation at the SC10 potential minimum corresponds to the ion gun emitting in the sunward direction. This suggests two possible explanations:

1) The net ion current is much smaller in magnitude than the telemetry indicates. The electron density near the spacecraft is higher on the sunward side because of photoemission. The beam current is being balanced by the photoelectron current, thus reducing the net current escaping the satellite.

2) Neutralization of the beam space-charge is taking place as it passes through the photoelectron cloud, shown schematically in Figure 22. This is a region of increased electron density, on the order of 100 cm-3. This might also reduce the net current escaping the satellite.

Insufficient information is available to resolve this problem. To do so would require better knowledge of the beam's parameters and behavior and more complete and accurate data on the ambient environment.

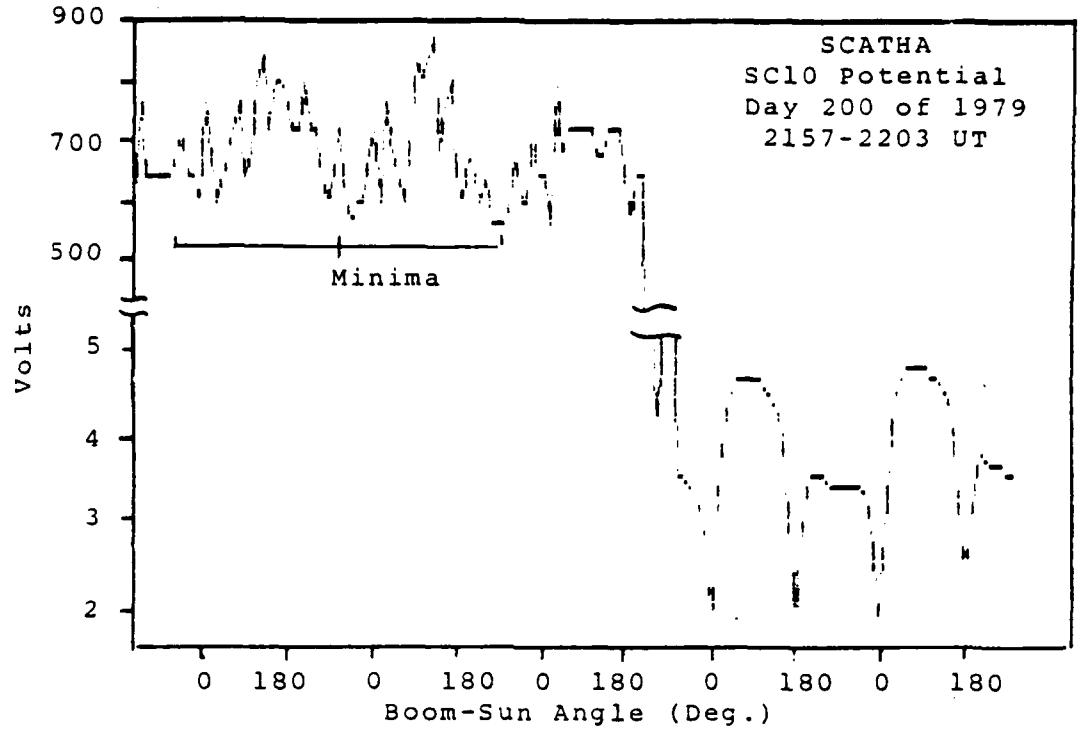

Figure 21. SC10 potential during transition into trickle mode.

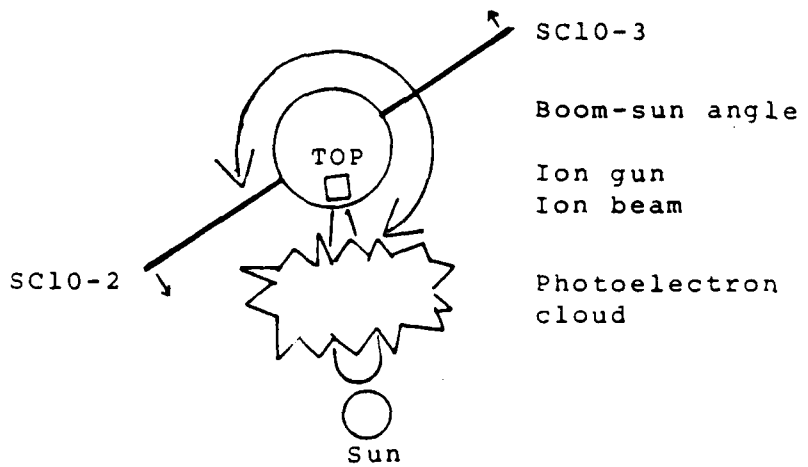

Figure 22. Schematic of spacecraft's orientation.

B. DAY 47

Observations for 16 February, 1979 (Day 47), are presented to illustrate the effects of ion gun operation on the spacecraft in a different plasma environment using similar (Day 200) beam parameters. During initial operations of the ion gun an experimental low current mode was used. In this mode, the main discharge went out and only the keeper operated. This resulted in a beam of 1 kV and 25 microamps. Unfortunately, the SC10 booms had not yet been deployed so those data are not available.

On this day the spacecraft was located near an altitude of 5.5 R_E between L = 5.7 and 6.5. Data used here were taken in the plasmasheet at local dawn. Figure 23 shows the distribution functions taken by the HI detector at 1447 UT. The calculated ambient particle densities and temperatures are displayed in Table III. The electron density moment is slightly higher than on Day 200.

1. High Voltage, High Current Mode

a. Observations

In Figure 24, the energy peak, which is close to the spacecraft potential, is plotted versus time. The turn on transient at 1449 UT again seems to show the satellite charging to near the beam energy and then stabilizing near -500 Volts after one minute. This is 200 volts more positive than the Day 200 operations. Figure 25, taken from the ion

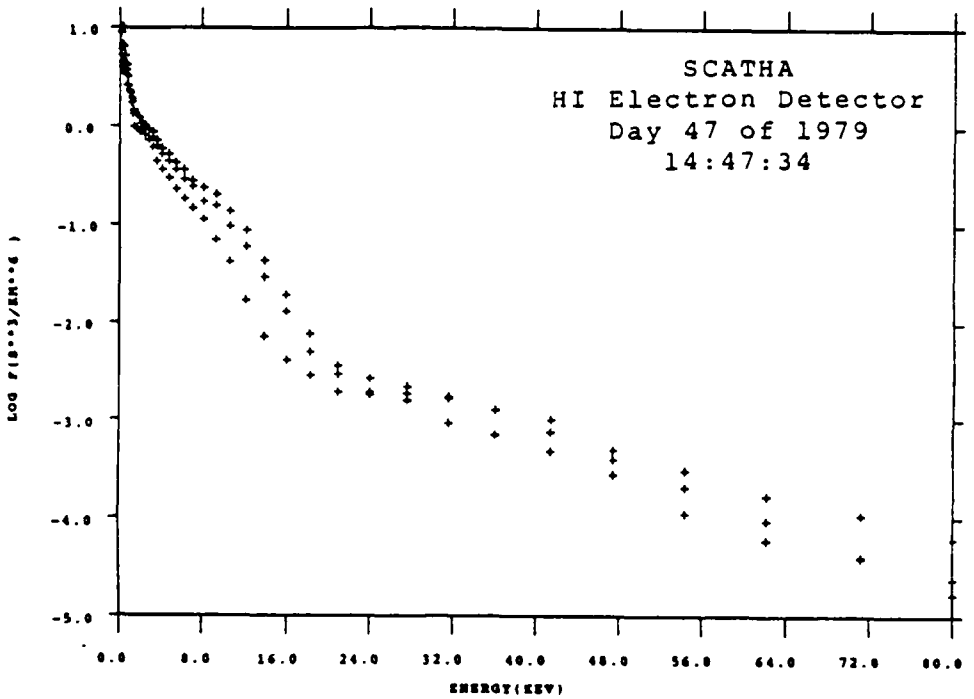

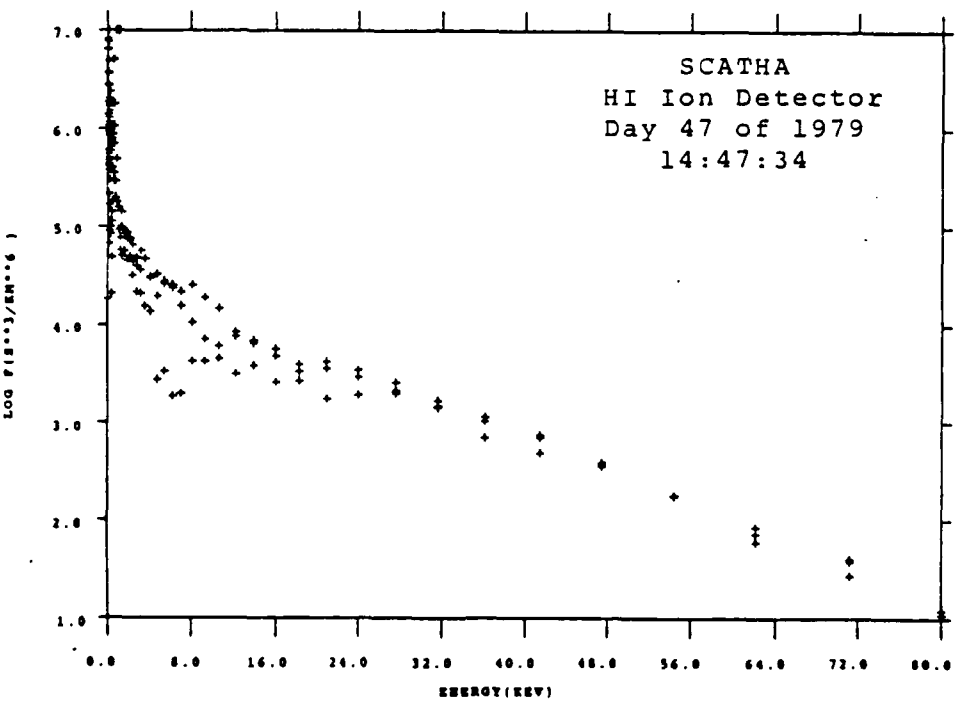

Figure 23. Electron and ion distribution functions, Day 47.

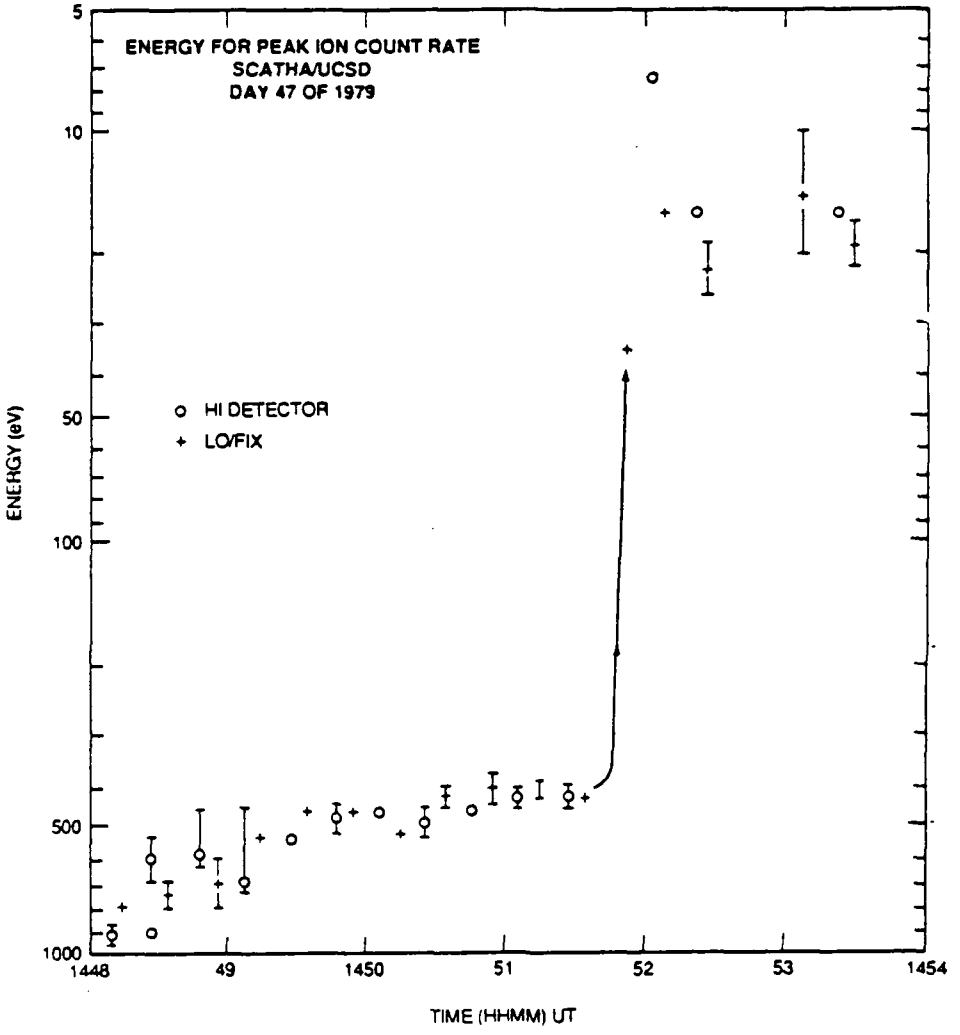

Figure 24. Energy peak vs time, Day 47.

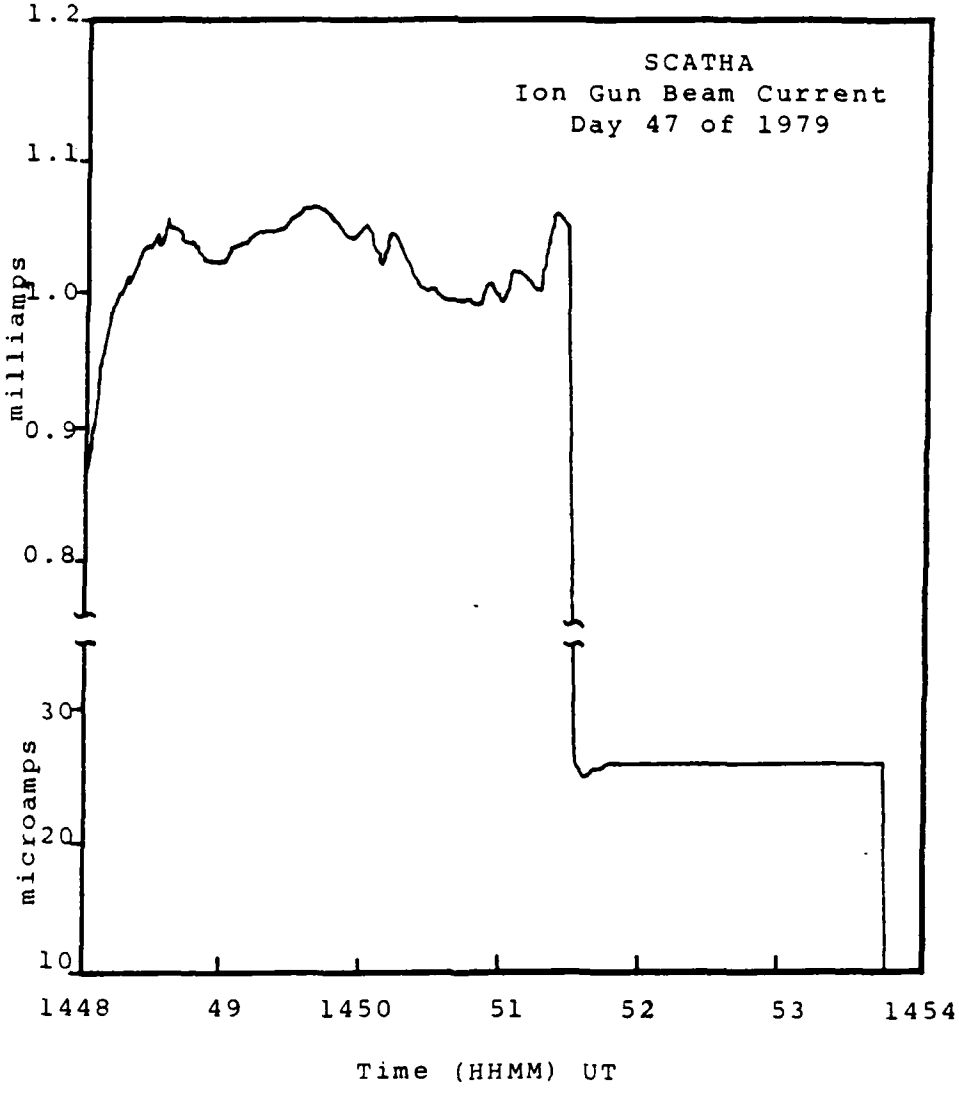

Figure 25. Ion gun beam current, Day 47.

gun telemetry for the same period, also shows the beam current increasing during the transient. After half a minute the beam steadies at current value near 1.05 milliamp. This suggests that although the potential does vary with the ion current, the transient is the response of the satellite system to a change in the input parameters.

TABLE III

DAY 47 PIECE-WISE MAXWELLIAN PARAMETERS

	Energy Range	Density (cm^{-3})	Temperature
Electrons:	20 - 100 eV	1.3	17.1 eV
	200 -1500 eV	0.24	370 KeV
	2 - 20 KeV	0.30	8.9 KeV
	20 - 80 KeV	0.02	11.8 KeV
Moments:	10 eV- 80 KeV	2.04	503 eV
Ions:	10 - 50 eV	0.12	15.8 eV
	50 - 500 eV	0.19	140 eV
	1 - 5 KeV	0.13	1.3 KeV
	5 - 80 KeV	0.19	14.8 KeV
Moments:	1 eV- 80 KeV	0.58	5.5 KeV

b. Analysis

The beam current is 0.5 mA lower than that used on Day 200, which could account for the more positive satellite potential. The ambient environment is slightly denser and hotter but the effect on the spacecraft potential during ion gun operations is less obvious and in this

case, probably minimal. The evidence presented so far suggests that the SCATHA spacecraft is very sensitive to changes in current balance during ion gun operation. That is, relatively small changes in current cause relatively large changes in potential.

On this day the spin modulation can be discerned directly from the plot of the ion particle data in Figure 24. This was difficult to do with the Day 200 data due to other fluctuations in the potential. Although the fluctuations are not as prevalent in this data as those seen on Day 200, they are probably present at a lower magnitude. This would make them difficult to detect because of the previously mentioned limitations of the SC9 particle detectors. There was no strong evidence of a second, higher energy peak above the charging peak. Thus, the beam would appear to be more stable and well behaved. This also suggests that the fluctuations in the spacecraft's potential and the appearance of a second peak in the distribution function near the beam energy are related.

2. <u>High Voltage, Low Current Mode</u>

At 1451 UT, the gun drops into the low current mode and a -10 to -20 Volt potential is seen. The net beam current is not modulated as on Day 200 because in this mode the ion current is determined by the gun perveance and 1 kV accelerating voltage. As on Day 200, however, net currents

in the 10 to 100 microamps range result in relatively small ($\Phi_{s/c}$ < 50V) potentials. Once the emitted current exceeds the current levels available through photoemission or from ambient plasma, the spacecraft will charge to a large negative potential, at times approaching the magnitude of the beam energy. The magnitude of the critical current should be roughly the same as the photocurrent in sunlight as this is the dominant positive current.

C. DAY 293

Data from operations on 20 October, 1979 (Day 293), are now presented to illustrate operation of the ion gun in eclipse. Eclipse events are of great value because they provide a variation of one of the dominant terms in the spacecraft current balance equation, the photoelectron flux. The effects of differential charging are therefore minimal and potential barriers and the transport of secondary electrons between spacecraft surfaces can be neglected (Olsen, 1983). When these data were taken, the spacecraft was in the plasmasheet at an altitude of 6.4 R_E and between L = 7.0 and 7.2. The spacecraft enters penumbra at 2042 UT and umbra at 2043 UT. Umbra exit is at 2141 UT. The data are summarized in the spectrogram of Figure 26. This example contains several gun on/off transitions and current-voltage combinations. The gun off transients at 2114, 2119, and 2129 are particularly interesting because of the way the ion peak

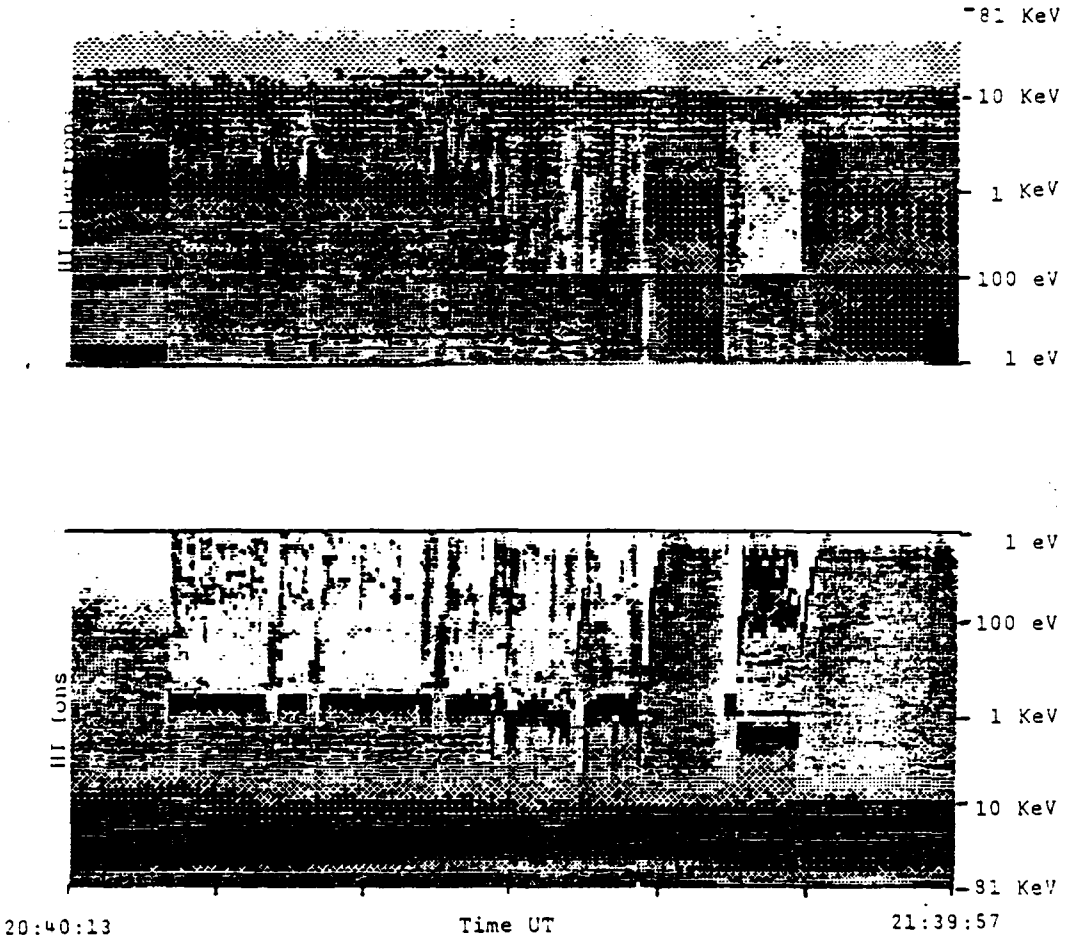

Figure 26. Spectrogram for ions and electrons, Day 293 of 1979.

trails off over a period of several minutes. Electron and ion distribution functions, taken from the HI detectors at 2045 UT, are shown in Figure 27. The calculated ambient density and temperature are presented in Table IV. This relatively quiet day provides substantially higher plasma densities than the previously presented experiments.

TABLE IV

DAY 293 PIECE-WISE MAXWELLIAN PARAMETERS

	Energy Range	Density (cm^{-3})	Temperature
Electrons:	50 - 150 eV	1.2	59.5 eV
	200 -1000 eV	2.9	586 eV
	2 - 6 KeV	5.7	655 eV
	10 - 80 KeV	0.036	11.4 KeV
Moments:	10 eV- 80 KeV	5.5	707 eV
Ions:	10 - 50 eV	0.063	20.6 eV
	100 - 500 eV	0.17	145 eV
	2 - 8 KeV	0.69	6.9 KeV
	10 - 80 KeV	1.2	12.5 Kev
Moments:	1 eV- 80 KeV	1.5	11.0 KeV

The SC10 potential and SC9 data are shown for the 2100 to 2130 UT period of unneutralized ion gun operation in Figure 28. Representative energy channel widths are shown with bars. As can be seen, the SC9 and SC10 data agree quite well and show the satellite potential fluctuating rapidly. The corresponding beam voltage and net beam current are shown in Figure 29. There is an obvious correlation between

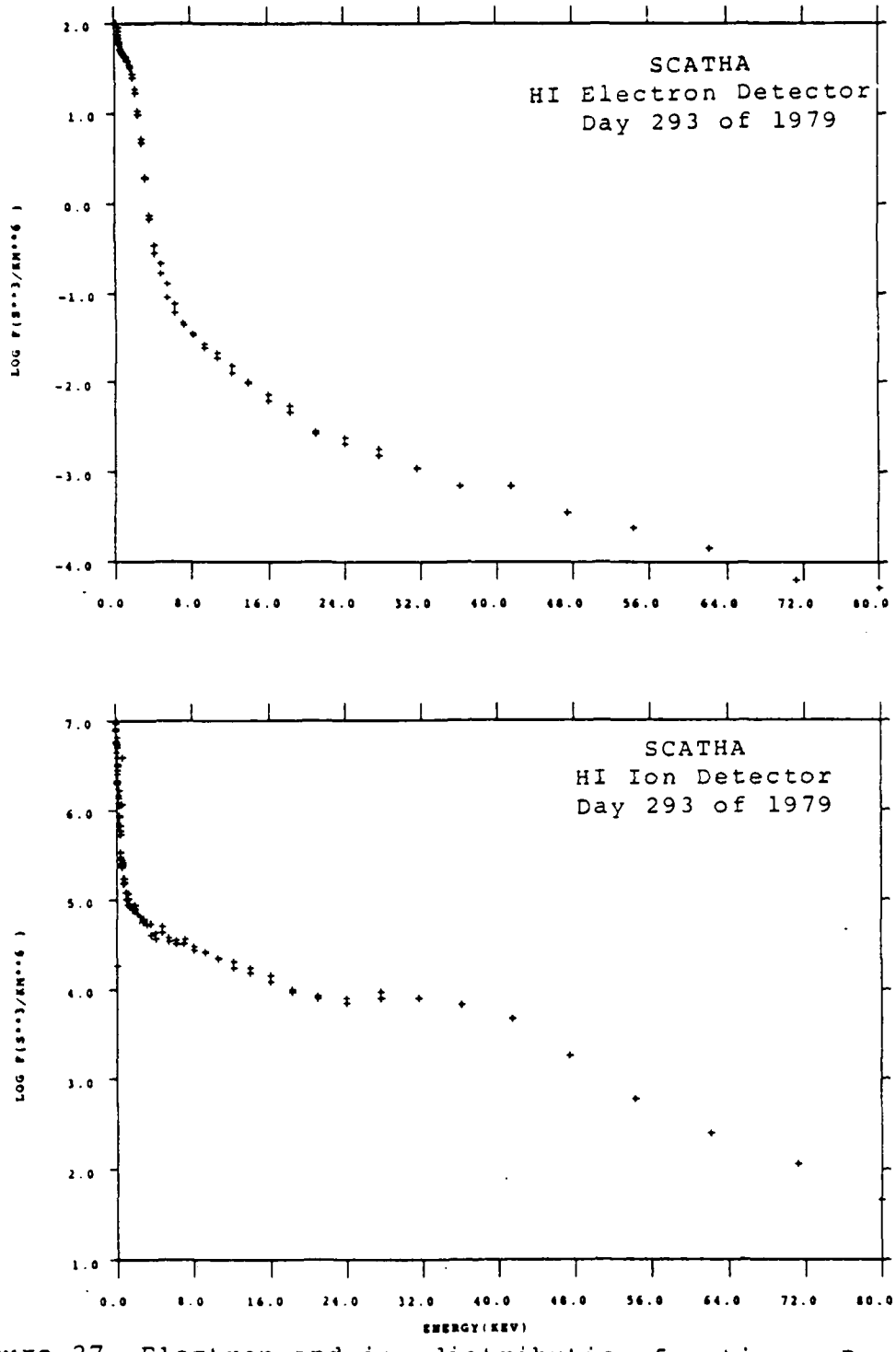

Figure 27. Electron and ion distribution functions, Day 293.

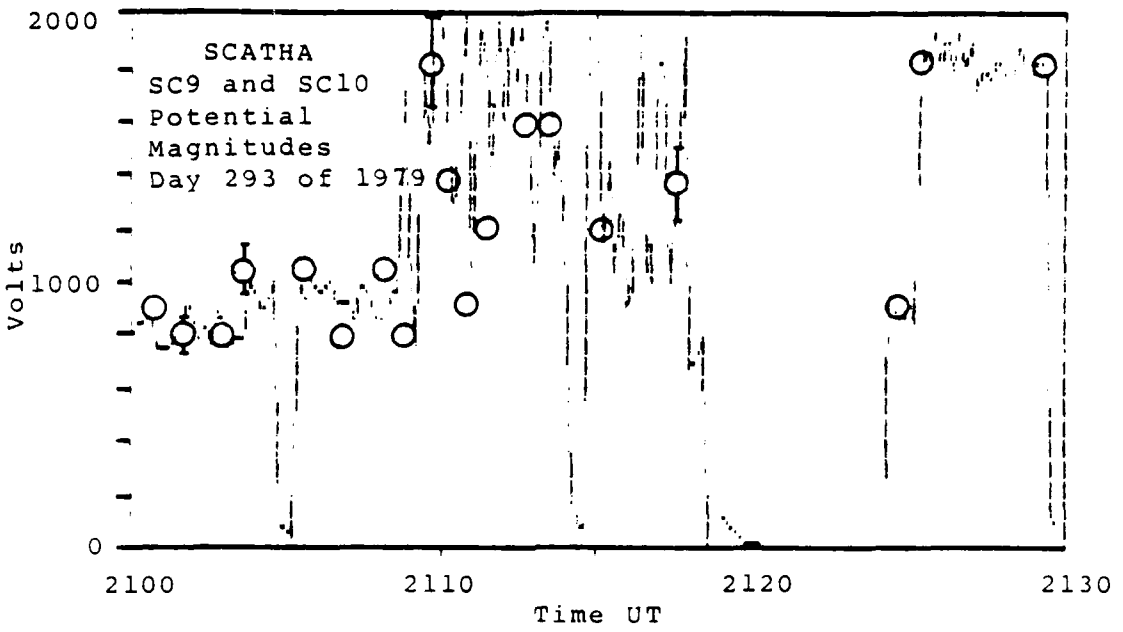

Figure 28. SC9 and SC10 potentials, Day 293.

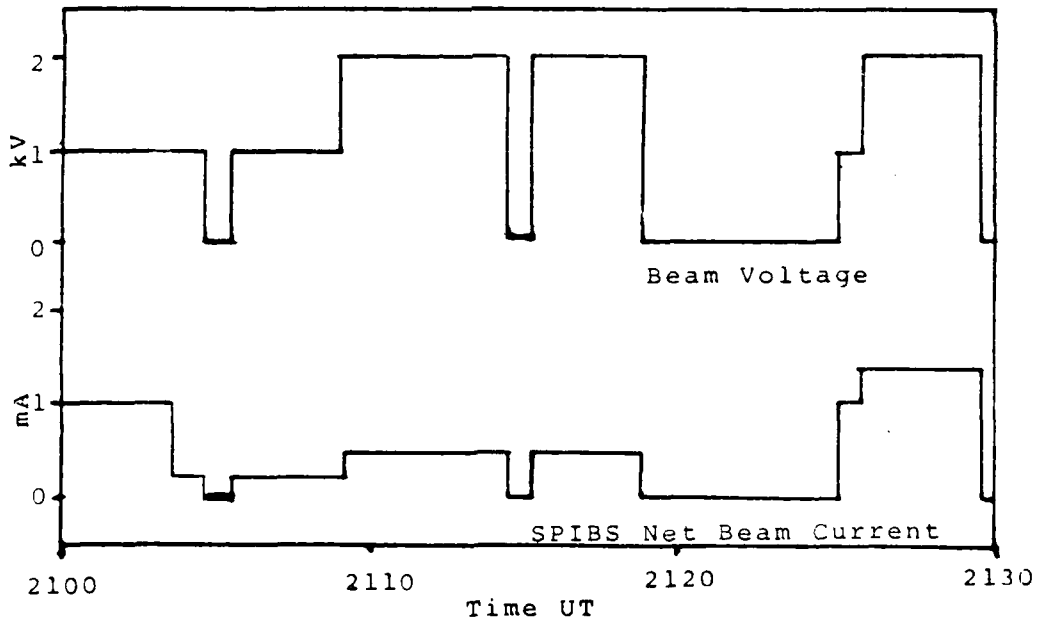

Figure 29. Ion gun beam voltage and beam current.

the beam parameters and the behavior of the satellite potential, summarized in Table V.

TABLE V

DAY 293 BEAM PARAMETERS AND SATELLITE POTENTIAL

NET BEAM CURRENT	BEAM VOLTAGE	SATELLITE POTENTIAL	FLUCTUATIONS
1.0 mA	1kV	-800 V	± 100 V
0.3 mA	1 kV	-900 V	± 100 V
0.5 mA	2 kV	-1500 V	± 500 V
1.5 mA	2 kV	-1800 V	± 100 V

During the time period from 2109 to 2114 UT, the ion gun is operating at a beam voltage of 2 kV and a net beam current of .5 mA. Examining the SC9 data for this period more closely showed the presence of secondary peaks in the distribution function at the beam energy (2 kV). Figure 30 shows the the ion distribution function from 21:12:45 to 21:17:17. These data were taken from the HI ion detector. Note that the gun was off from 21:13:49 to 21:14:37, as seen by the absence of any peaks in the distribution function. The most obvious 2 kV peaks are at 2i:13:01, 21:14:53, and 21:16:45. The detector head angle was fixed at near 100 degrees and the corresponding particle pitch angle is given in the table. During the 2125-2130 UT time period, the ion

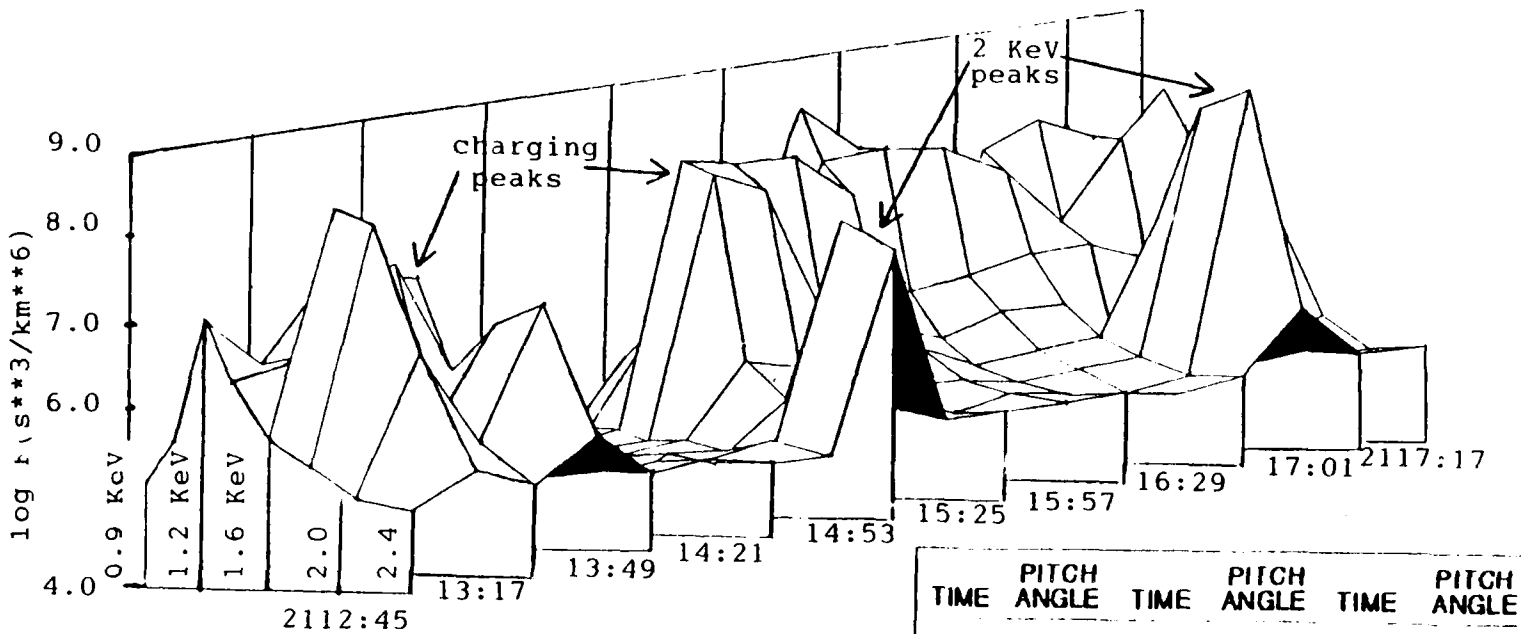

TIME	PITCH ANGLE	TIME	PITCH ANGLE	TIME	PITCH ANGLE
2112:45	93	2114:21	64	2115:57	77
2113:01	85	2114:37	67	2116:13	91
2113:17	57	2114:53	97	2116:29	75
2113:33	82	2115:09	77	2116:45	97
2113:49	96	2115:25	58	2117:01	70
2114:05	94	2115:41	89	2117:17	62

DETECTOR ANGLE = 100 DEGREES

Figure 30. Time variation of the HI ion distribution function.

gun is operated at 2 kV and a net current of 1.5 mA. The magnitude of the fluctuations in the SC10 data is much smaller than seen with the 2 kV, .5 mA beam.

Figure 31 shows a series of four distribution functions from 21:23:57 to 21:26:21. The top plot shows the HI ion distribution for gun off. Shifting the unaccelerated ion distribution curve up 800 eV (invoking Liouville's Theorem, or phase space invariance) brings the first and second plots into agreement, indicating a satellite potential of -800 Volts at 21:24:29, when the gun is on at 1 kV and 1 mA. The subsequent energy scan, plot three, is for the same gun parameters and is similar to the second plot. The difference is the boxed data point at 1 KeV. This data point suggests returned 1 KeV ions from the gun or scattering of the beam. The last plot for 2 kV and 1.5 mA, indicates a satellite potential of -1800 Volts. The two boxed data points are again interpreted as a result of spreading of the velocity distribution of beam ions. The circled data point most likely represents spacecraft generated ions (Norwood, 1988). Figure 32 shows the corresponding distributions for the HI electrons. If our interpretation of variations in satellite potential are correct, equivalent shifts in energy should make it possible to bring agreement to these curves. This works for 1 kV but not for 2 kV, where a $\Delta\Phi$ of 1.5 kV is needed for the electrons vice 1.8 kV for the ions. The

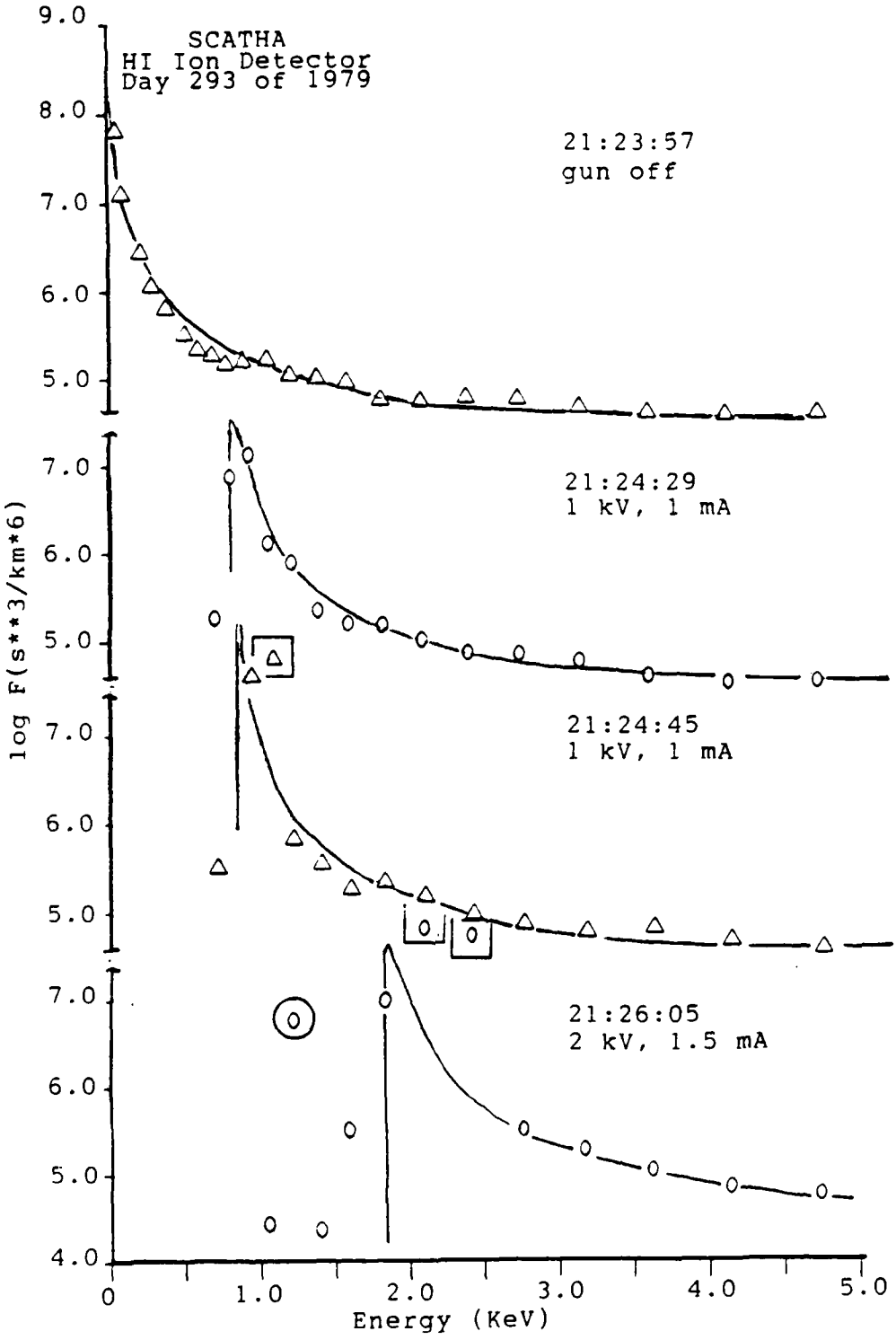

Figure 31. Ion distribution functions, Day 293.

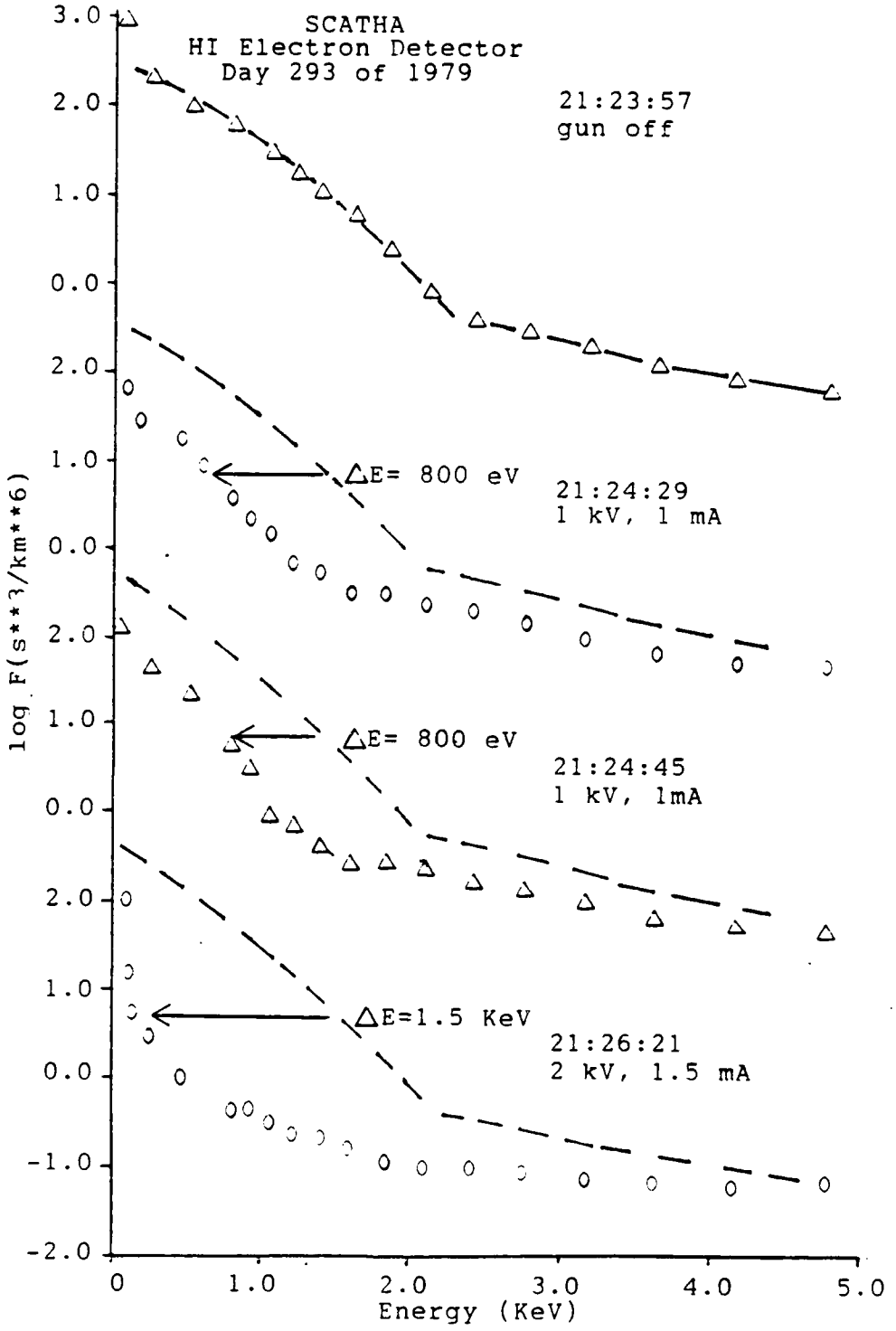

Figure 32. Electron distribution functions, Day 293.

explanation of this last discrepancy is uncertain. It may be due to a change in the ambient electron density. A change on the order of 10% would be sufficient.

In comparing the data taken on this observation day to that taken on Day 47 for a 1 kV, 1 mA beam, it is obvious that the spacecraft stabilized at a higher (less negative) potential. Table VI compares the beam parameters for Day 47 and Day 293.

TABLE VI

ION BEAM PARAMETERS, DAY 47 AND DAY 293

Parameter	Day 47 (1450 UT)	Day 293 (2100 UT)
Beam Voltage	1 kV	1 kV
Beam Current	1.05 mA	1.08 mA
e^- Density	2.04 cm^{-3}	5.50 cm^{-3}
e^- Temperature	503 eV	707 eV
Spacecraft Potential	-500 V	-800 V

The ion gun parameters are the essentially the same; the calculated electron densities differ by a factor of two. Changes in the instrument response with time will affect the validity of this comparison, but it appears consistent with differences in local time and magnetic activity on these days. The other obvious difference between is that the Day

293 operations take place in eclipse. It is likely that photoelectrons play a significant role in determining the spacecraft potential during ion gun operations. One possible effect is that in sunlight, the ion beam space-charge is partially neutralized by the electrons of the photosheath. We would therefore expect the satellite to charge nearer the magnitude of the beam voltage in eclipse than in sunlight, excluding the very unstable modes of operation. A more extended survey of unneutralized ion gun operations in eclipse at similar beam parameters would be the next logical step in this study.

The additional feature which appears in eclipse data is a delay in the return to the equilibrium potential. The SC10 potential is plotted for the gun off transition in Figure 33. This segment is typical of the times for Day 293 when the gun is switched off. Initially, there is a rapid decay in the SC10 potential, and hence, the spacecraft potential, followed by an overshoot and a small rise, and finally a minute long decay towards zero. This can be seen on the spectrogram as the trailing off of the ion peak to near zero energy when the ion gun is switched off. From the initial decay, a maximum value for the spacecraft frame capacitive time constant on the order of 1 second was obtained. The last decay has a time constant of 10 to 20 seconds. The

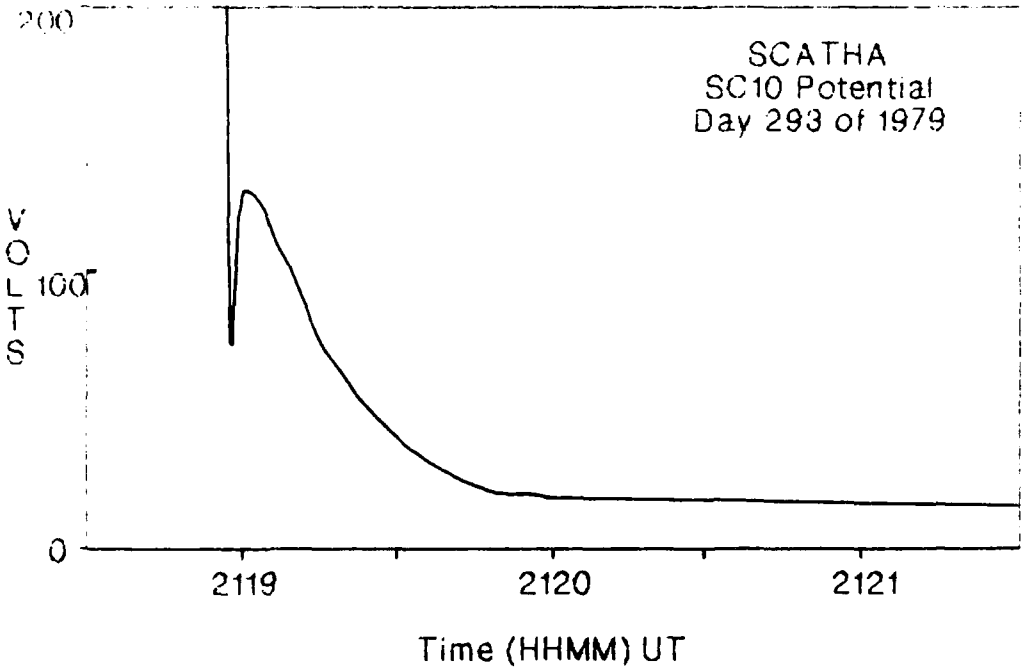

Figure 33. SC10 gun off transition.

last set of observations show an excellent example of this effect.

E. DAY 295

1. Observations

Data from ion gun operations on 22 October, 1979 (Day 295), are presented to illustrate details of the spacecraft response to ion gun transitions in eclipse. The spacecraft enters penumbra at 2002 UT and umbra at 2004 UT. Umbra exit is at 2058UT. Ion and electron distribution function for 0 to 80 KeV are shown in Figure 34. Data were taken from the HI detectors at 19:54:21. Table VII gives the calculated ambient densities and temperatures. As on Day 293, this is a quiet day, with relatively high ambient density.

TABLE VII

DAY 295 PIECE-WISE MAXWELLIAN PARAMETERS

	Energy Range	Density (cm^{-3})	Temperature
Electrons:	20 - 100 eV	2.0	25.2 eV
	100 -1000 eV	2.7	420 eV
	1 - 10 KeV	4.8	940 eV
	10 - 80 KeV	0.038	15.2 Kev
Moments:	20 eV- 80 KeV	6.0	883 eV
Ions:	20 - 400 eV	0.17	111 eV
	400 -1000 eV	0.12	735 eV
	1 - 10 KeV	0.74	8.7 KeV
	10 - 80 KeV	1.1	13.2 KeV
Moments:	1 eV- 80 Kev	1.3	10.1 KeV

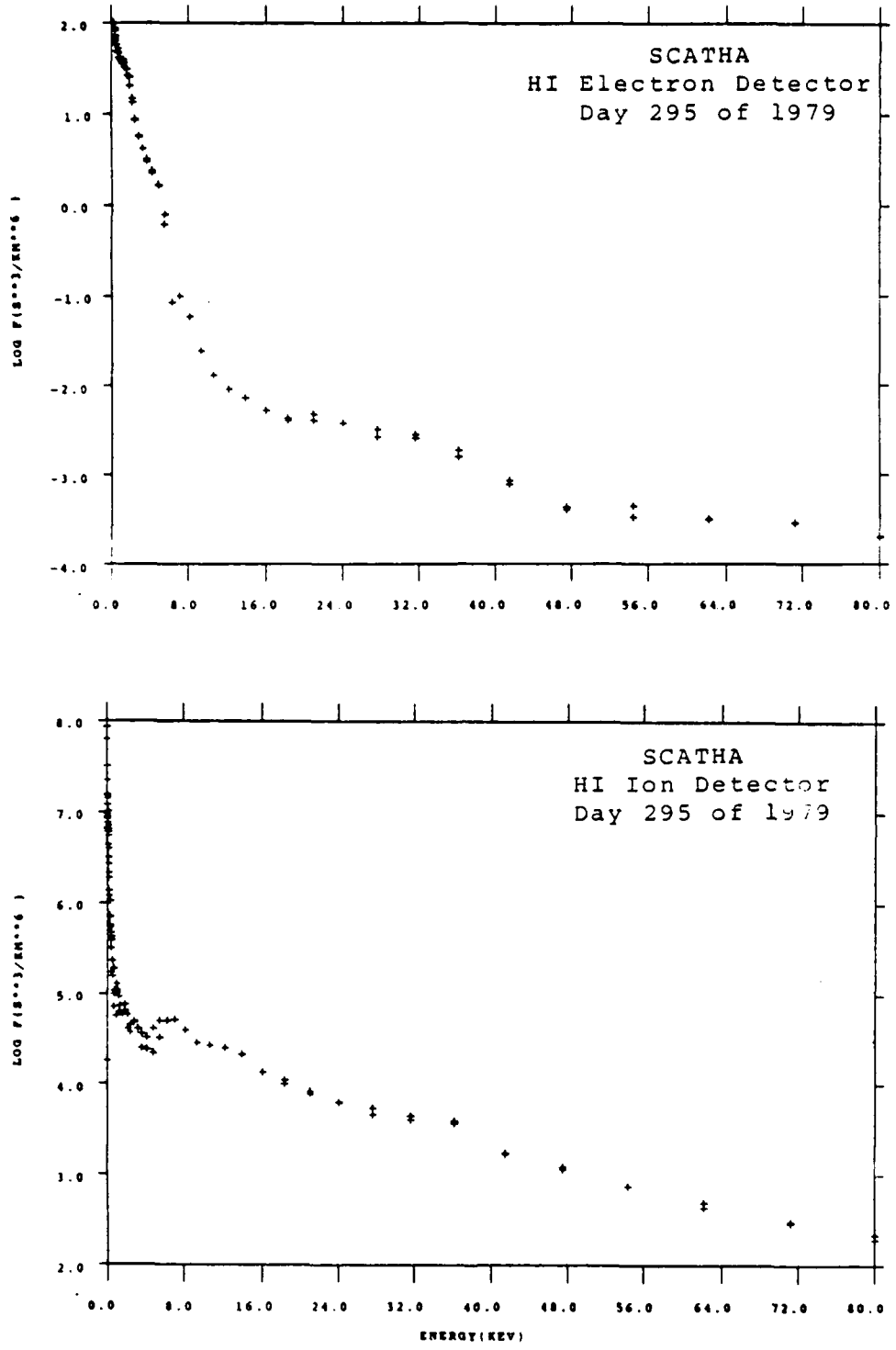

Figure 34. Electron and ion distribution functions, Day 295.

The SC9 data are summarized in spectrogram form in Figure 35. The decay spacecraft potential at gun off is clearly seen in the trailing off of the ion peak at 2037 UT. The energies for the ion charging peaks for three minutes after the ion gun is switched off are plotted in Figure 36, along with the SC10 potential. The response is similar to that found on Day 293. This behavior is seen repeatedly in this data set.

2. Analysis

The time behavior of the satellite charging indicates differential charging. Figure 36 illustrates the two different charging processes in action. First, the structure potential changes rapidly in response to the cessation of ion gun operation. This process is determined by the pico-Farad capacitance of the spacecraft to plasma. The second process is more complex and involves the differentially charged non-conducting surfaces. The associated capacitance is micro-Farads. The suggested sequence of events is shown in Figure 37. Initially (gun on), the mainframe is near -1300 Volts, as observed. The insulated surfaces are slowly discharging back to near zero Volts, their eclipse equilibrium. Typically, these surfaces are several hundred volts less negative than the frame potential. At gun off, the frame potential drops to near zero and the the insulator potential is pushed towards a

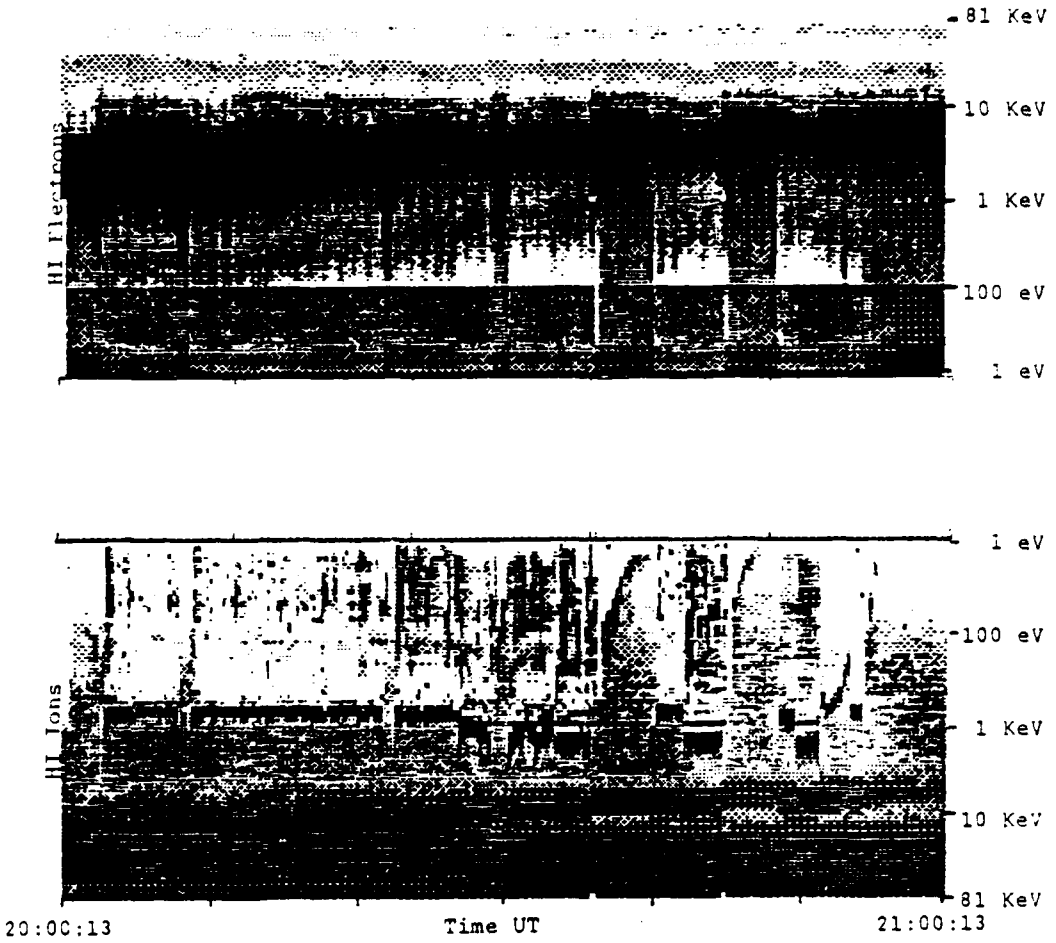

Figure 35. Spectrogram for ions and electrons, Day 295 of 1979.

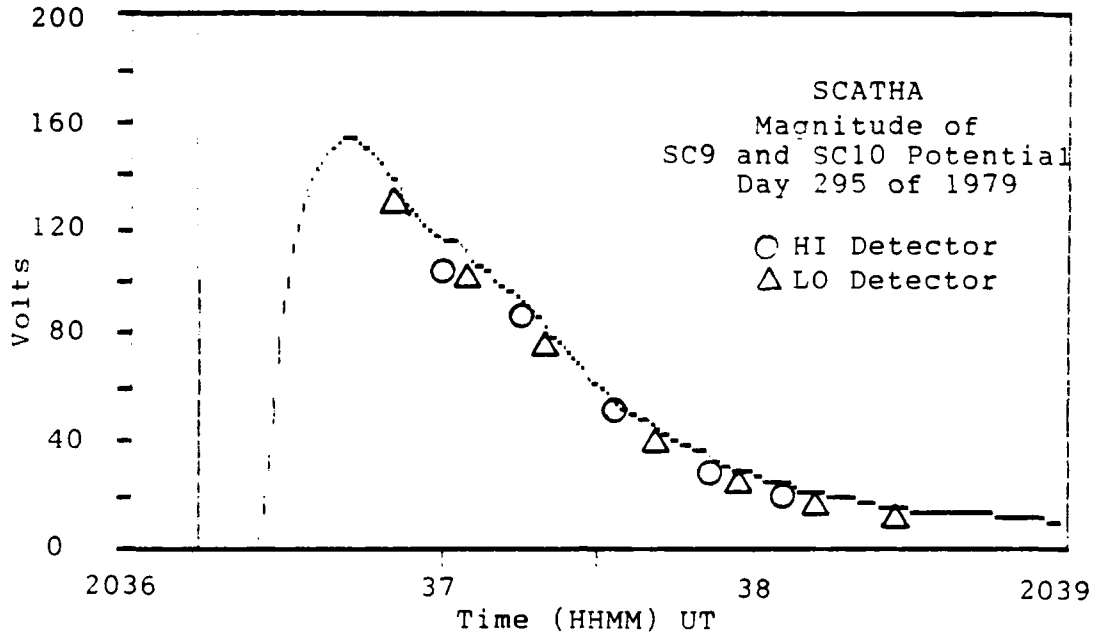

Figure 36. SC9 and SC10 gun off transient.

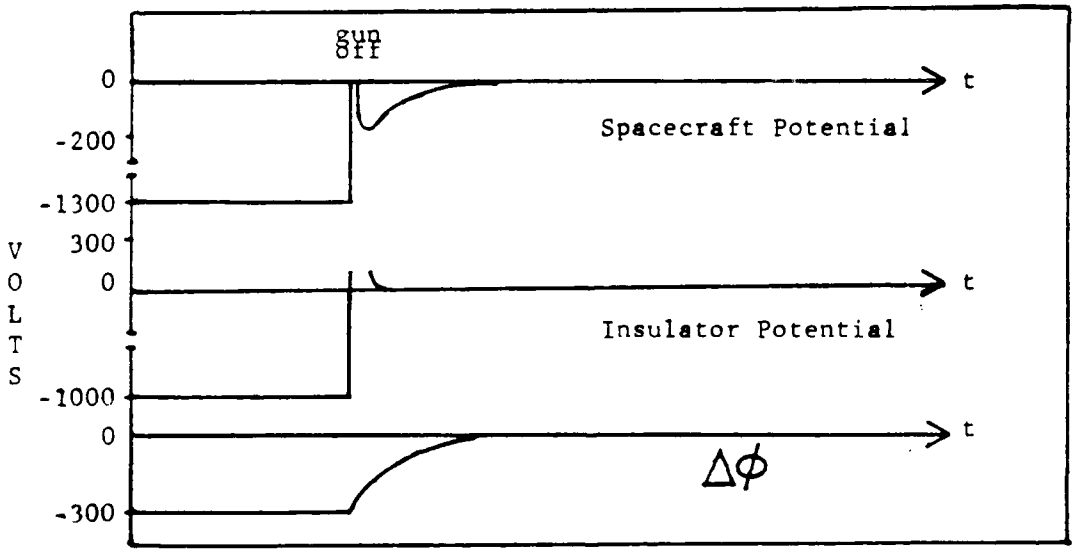

Figure 37. Spacecraft and insulator potential.

positive value. The positive surfaces are not stable and attract a large negative current. The system, still seeking equilibrium, responds by swinging the frame potential negative again. The differential potential then decays exponentially with a time constant on the order of 10 to 100 seconds, allowing the mainframe to approach zero Volts.

IV. DISCUSSION

It has been suggested (Stannard et al., 1980) that the SCATHA unneutralized ion beam is extremely space charge limited. The referenced analysis was based upon simple space-charge limited diode theory and brings the predicted satellite voltages into rough agreement with experiment. The predicted net ion beam currents escaping from the near satellite region are on the order of 50 to 60 microamps. The photoelectron current could have a significant effect, as observed in this thesis, if the ion currents are of this magnitude. Also, the data in Table V show the magnitude of the satellite potential increasing when the 1 kV beam current is decreased from 1 mA to .3 mA. Therefore, space-charge limiting of the ion beam is consistent with the observations made in this thesis.

When the injected current exceeds the space-charge limiting current, the system becomes inherently unstable. There is no simple analytical framework that provides an adequate description of the complex time-dependant particle bunching and reflection that occur. This phenomena has been studied using numerical particle simulation codes (Bridges and Birdsall, 1963). The instability predicted resembles the fluctuations seen during operation of the ion gun and

extends the space-charge limited diode model one step further.

Qualitatively, what may be happening is that as the injected current from the gun exceeds the space charge limit, a virtual anode is formed. Some charges are reflected back to the injection plane. This reflection creates a charge bunch that further traps and reflects charge injected at later times. Simultaneously, the charges that were injected prior to the first reflection continue to exit. The electrostaic potential of the virtual anode region decreases because charge is exiting the region in both directions. The charges injected at still later times are no longer trapped and propagate out, increasing the potential. The oscillation then repeats. The oscillations are not sinusoidal and their frequency does not scale linearly with the beam plasma frequency. The resulting oscillations in the net current exiting from the satellite region may account for the potential fluctuations. The second peak in the distribution function may be explained as ions from the gun randomly intercepting trajectories back to the spacecraft because the beam never comes to an equilibrium state.

V. CONCLUSION

Examinations of daylight ion emission events suggest that a trickle (no accel voltage) current less than 80 microamps is effective for potential control. For the relatively typical observation day studied in this thesis, the potential was held to near zero. Trickle mode, however, did not reduce the small (about 1 Volt) frame potential modulation caused by the different photoemissive properties of the exposed grounded conducting surfaces. The low current mode was successful in reducing the satellite potential magnitude to less than 50 Volts.

Ion gun operation at 1 and 2 kV induced negative satellite potentials less than the magnitude of the beam energy. This is attributed to space-charge effects, which may also be responsible for the fluctuations in the potential. A beam current of .3 to 1 mA for a 1 kV beam appears to be close to optimum; the induced potential is close to the magnitude of the beam energy and the fluctuations are small in magnitude.

NASCAP (see Appendix) modeling of similar ion gun operation as examined in this thesis resulted in the spacecraft charging to a value equal to the beam energy down to a beam current near 25 microamps (Olsen, private

communication, 1988). NASCAP has been thoroughly validated as an accurate model of spacecraft charging response but it does not take into account space charge effects or other aspects of charged particle beam physics. This also suggests that the beam itself is the source of the effects described in this thesis.

In general, the spacecraft charging system appeared very sensitive to small deviations in the current balance. Operations at 1 kV in high and low current modes suggest a critical current above which the spacecraft will charge to near beam energy. If the beam current is less than the critical current, the spacecraft will charge to a much lower (less negative) potential. This was also indicated using the NASCAP code (Olsen, private communbication, 1988), which yielded a value near 25 microamps for the critical current. This is consistent with current balance theory in that it is of the same order as the estimated photocurrent from the spacecraft.

A fundamental limitation of this thesis is the lack of accurate data concerning the composition, energy, and mass of the ambient particle environment. Detailed analysis of the behavior of the ion beam is greatly complicated, if not impossible. This exemplifies the need for better and more complete instrumentation on future satellite flights.

The existence of differential charging was inferred during ion gun operation in eclipse and may be expected for most any induced charging event. This was also suggested using NASCAP. While no direct observations of barrier formation can be made for the observation times used in this thesis, the existance of one is typical for the estimated differential charging level and environments observed in this thesis. The formation of a barrier would increase the density of electrons near the spacecraft by not allowing their escape. Since the density and energy of the ambient environment would affect the strength of the barrier and hence the density of trapped electrons, interaction of the ion beam with the barrier-trapped electrons may affect the equilibrium value of the spacecraft potential. The dependendence of the spacecraft potential during ion gun operations on differential charging could be further analyzed by examining the data collected by the SC1 experiment surface potential monitors.

In conclusion, the interaction of a spacecraft, an emitted ion beam, and the ambient environment is very complex and difficult to unravel. More accurate knowledge of the environment and better beam diagnostics are required to fully analyze the physics. However, much data already exists which may provide at least a fundamental understanding and suggestions for future experiments.

APPENDIX

NASCAP

The NASA Charging Analyzer Program (NASCAP) is a three dimensional code which is capable of establishing an object in a 16 x 16 x 32 grid and solving for the potentials and currents to spacecraft surfaces in magnetospheric environments. Material placement on the surface of the spacecraft is modeled as well as the interior electrical connections. Particle trajectories reaching the detectors can be traced, including those from onboard positive and negative emitters, in order to estimate escaping flux and to simulate active control of satellite potentials. The complex three-dimensional effects can more easily be studied using the codes extensive graphic capability.

Simple shapes, such as cubes or slices of cubes, are used as building blocks to model more complex objects. Particle fluxes of the ambient environment can be input as single or double Maxwellians or as actual observed spectra. The code accounts for incident electrons and protons, backscattered and secondary electrons, secondary electrons due to protons, and photoelectrons.

The NASCAP code computes alternate solutions to Poisson's equation and calculations of particle motion and

charge deposition in a series of time steps appropriate to the specific problem. It is assumed that the charging process proceeds through a series of equilibrium states. NASCAP and its underlying physical principles have been validated by comparing prediction to experimental and actual spacecraft data. NASCAP has proven itself a very useful predictive and analytic tool.

So that particle trajectories may be calculated out to large distances, NASCAP computations are carried out in a series of nested grids. Each successive grid has twice the spacing of the previous grid with the spacecraft being in the innermost grid. This thesis uses the "one-grid" NASCAP model which uses considerably less computer time and memory but shows a similar charging response to the more detailed versions. The spacecraft's main body is represented as a right octagonal cylinder. Grid resolution is 19.6 cm which allows the model to reproduce SCATHA's geometrical features very well.

Each of the 15 distinct exposed surface materials used in this model is specified by the value of 14 parameters. Experimentally measured values were used if available, otherwise estimates based on the properties of similar materials were used.

The NASCAP code can recognize plasma spectra in the form of a single and a double Maxwellian. In general, the double

double Maxwellian is a better representation of the non-Maxwellian actual environment.

Particle emitters are modeled in NASCAP by specifying the location of the emitter on the spacecraft and the energy and angular width of the beam. The beam particles are tracked in the satellite sheath field until they escape through a distant boundary or return to a specific cell on the spacecraft.

(Rubin et al, 1980; Stannard et al, 1980)

LIST OF REFERENCES

Aggson, T. L., B. G. Ledley, A. Egeland, I. Katz, "Probe Measurements of DC Electric Fields," Proceedings of the 17th ESLAB Symposium on Spacecraft/ Plasma Interactions and Their Influence on Field and Particle Measurements, ESA SP-198, pp 13-17, 1983.

Banks, P. M., A. C. Fraser-Smith, B. E. Gilchrist, K. J. Harker, L. R. O. Storey, P. R. Williamson, "New Concepts in Ionospheric Modification ," Stanford University, Dept. of Electrical Engineering, Space, Telecommunications, and Radioscience Laboratory, Technical Report No. D131-1, 1987.

Bridges, W. B. and C. K. Birdsall, "Space-Charge Instabilities in Electron Diodes. II," Journal of Applied Physics, v. 34, pp 2946-2955, October 1963.

Chappell, C. R., "The Convergence of Fact and Theory on Magnetospheric Convection," Correlated Interplanetary and Magnetospheric Observations, D. Reidel Publishing Company, 1974.

Craven, P. D., R. C. Olsen, J. Fennell, D. Croley, T. Aggson,"Potential Modulation on the SCATHA Spacecraft," Journal of Spacecraft and Rockets, v. 24, pp. 150-157, March-April 1987.

DeForest, S. E., "Spacecraft Charging at Synchronous Orbit," Journal of Geophysical Research, v. 77, pp. 651-659, February 1972.

Fennel, J. F., "Description of P78-2 (SCATHA) Satellite and Experiments," IMS Source Book, pp. 65-78, AGU, Washington D. C., 1982.

Gavrilov, F. , A. Myasnikov, G. Zhadan, G. Orlova, M. Strokin, "Some Results of Flight Tests of an Ion-Engine Model Using Surface Ionization of Tungsten," Translated from Kosmicheskie Issledovaniya, v. 11, pp. 140-144, January-February, 1973.

Grard, R., Knott, K., and Pedersen, A., "Spacecraft Charging Effects," Space Science Reviews, v. 34, pp. 289-304, 1983.

Gussenhoven, M. S., and E. G. Mullen, "Geosynchronous Environment for Severe Spacecraft Charging," Journal of Sapcecraft and Rockets, v.20, pp.26-34, January-February 1983.

Hunter, R. E,, R. O. Bartlett, "Cesium Contact Ion Microthruster Experiment Aboard Applications Technology Satellite (ATS)-IV," Journal of Spacecraft and Rockets, v. 6, pp. 968-970, 1969.

Jones, S., J. Staskus, D. Byers, "Preliminary Results of SERT II Spacecraft Measurements Using Hot Wire Emissive Probes," NASA TM X-2083, November 1970.

Katz, I., M. Mandell, "Differential Charging of High-Voltage Spacecraft: The Equilibrium Potential of Insulated Surfaces," Journal of Geophysical Research, v. 87, pp. 4533-4541, June 1982.

Kintner, P. M., M. C. Kelley, "Ion Beam Produced Plasma Waves Observed by the δn/n Plasma Wave Receiver During the Porcupine Experiment," Advanced Space Research, v. 1, pp. 107-115, 1981.

Lai, S. T., H. A. Cohen, T. L. Aggson, W. J. McNeil, "Boom Potential of a Rotating Satellite in Sunlight," Journal of Geophysical Research, v. 91, pp. 12,137-12,141, November 1986.

Lai, S. T., H. A. Cohen, T. L. Aggson, W. J. McNeil, "The Effect of Photoelectrons on Boom-Satellite Potential Differences During Electron Beam Ejection," Journal of Geophysical Research, v. 92, pp. 12,319-12,325, November 1987.

Masek, T. D. and Cohen, H. A., "Satellite Positive-Ion Beam System, "Journal of Spacecraft and Rockets, v. 15, pp. 27-33, January and February 1978.

Masek, T. D., "Satellite Positive Ion Beam System," Final Report, AFGL-TR-78-0141, 1978.

McIlwain, C. E. and E. C. Whipple, "The Dynamic Behavior of Plasmas Observed Near Geosynchronous Orbit," Transactions on Plasma Science, v. PS-14, pp. 874-890, December 1986.

McPherson, D. A., D. P. Cauffman, CAPT. W. Schober, "Spacecraft Charging at High Altitudes--The SCATHA Satellite Program," AIAA Paper 75-92, 1975.

Mullen, E. G., M. S. Gussenhoven, and D. A. Hardy, "SCATHA Survey of High-Level Spacecraft Charging in Sunlight," Journal of Geophysical Research, v.91, pp. 1474-1490, February 1986.

Norwood, C. W., Ions Generated On or Near Satellite Surfaces, MS Thesis, Naval Postgraduate School, June 1988.

Olsen, R. C. and C. K. Purvis, "Observation of Charging Dynamics," Journal of Geophysical Research, v. 88, pp. 5657-5667, July 1983.

Olsen, R. C., "Experiments in Charge Control--ATS-5 and ATS-6," Journal of Spacecraft and Rockets, v. 22, pp 254-264, May-June 1985.

Olsen, R. C., UAH Final Report on Grant NAG3-620 with NASA LeRC, May 1987.

Purvis, C., R. Bartlett, "Active Control of Spacecraft Charging," Progress in Astronautics and Aeronautics, v. 71, pp. 299-317, 1980.

Rubin, A. G., Katz, I., Mandell, M., Schnuelle, G., Steen, P., Parks, D., Cassidy, J., Roche, J., "A Three Dimensional Spacecraft-Charging Computer Code, "Progress in Astronautics and Aeronautics, v. 71, pp. 318-336, 1980.

SCATHA Handbook, UCSD/AF SCATHA F04701-77-C-0062, 1980.

Stannard P. R., I. Katz, M. Mandell, J. Cassidy, D. Parks, M. Rotenberg, P. Steen, "Analysis of the Charging of the SCATHA (P78-2) Satellite," NASA CR-165348, 1980.

Whipple, E. C., "The Equilibrium Electric Potential of a Body in the Upper Atmosphere," NASA Rep. X-615-65-296, 1965.

Yeh, H. C., M. S. Gussenhoven, "The Statistical Electron Environment for Defense Meteorological Satellite Program Eclipse Charging," Journal of Geophysical Research, v. 92, pp. 7705-7715, July 1987.

INITIAL DISTRIBUTION LIST

		No. Copies
1.	Defense Technical Information Center Cameron Station Alexandria, Viriginia 22304-6145	2
2.	Library, Code 0142 Naval Postgraduate School Monterey, California 93943-5002	2
3.	Department Chairman, Code 61 Department of Physics Naval Postgraduate School Monterey, California 93943	2
4.	Dr. R. C. Olsen, Code 61OS Department of Physics Naval Postgraduate School Monterey, California 93943	20
5.	Dr. S. Gnanalingam, Code 61GM Department of Physics Naval Postgraduate School Monterey, California 93943	1
6.	Dr. J. Quinn Dept. 91-20, Bldg 255 Lockheed Palo Alto Research Laboratory 3251 Hanover St. Palo Alto, California 94304	1
7.	Ms. D. E. Donatelli Space Physics Division Air Force Geophysics Laboratory/PH Hanscom AFB, Massachusetts 01731	1
8.	D. Klumpar Dept. 91-20, Bldg 255 Lockheed Palo Alto Research Laboratory 3251 Hanover St. Palo Alto, California 94304	1
9.	Dr. W. Peterson Dept. 91-20, Bldg 255 Lockheed Palo Alto Research Laboratory 3251 Hanover St. Palo Alto, California 94304	1

10. Dr. E. Shelley 1
Dept. 91-20, Bldg 255
Lockheed Palo Alto Research Laboratory
3251 Hanover St.
Palo Alto, California 94304

11. Dr. R. Sagalyn 1
Space Physics Division
Air Force Geophysics Laboratory/PH
Hanscom AFB, Massachusetts 01731

12. Mr. G. Mullen 1
Space Physics Division
Air Force Geophysics Laboratory/PH
Hanscom AFB, Massachusetts 01731

13. Dr. S. Lai 1
Space Physics Division
Air Force Geophysics Laboratory/PH
Hanscom AFB, Massachusetts 01731

14. Dr. B. Burke 1
Space Physics Division
Air Force Geophysics Laboratory/PHA
Hanscom AFB, Massachusetts 01731

15. Dr. N. Maynard 1
Space Physics Division
Air Force Geophysics Laboratory/PH
Hanscom AFB, Massachusetts 01731

16. Mr. H. A. Cohen 1
W. J. Schafer Associates
1901 North Fort Meyer Drive
Arlington, Virginia 22209

17. Mr. R. Gracen Joiner 1
Office of Naval Research, Code 1114
800 North Quincy Street
Arlington, Virginia 22217-5000

18. Dr. H. C. Koons 1
Space Science Laboratory
The Aerospace Corporation, M2/260
P.O. Box 92957
Los Angeles, California 90009

19. Dr. J. Fennell 1
Space Science Laboratory
The Aerospace Corporation, M2/260
P.O. Box 92957
Los Angeles, California 90009

20. Dr. J. Roeder 1
Space Science Laboratory
The Aerospace Corporation, M2/260
P.O. Box 92957
Los Angeles, California 90009

21. Dr. E. C. Whipple 1
Center for Astrophysics and Space Science
University of California at San Diego
La Jolla, California 92093

22. Dr. C. E. McIlwain 1
Center for Astrophysics and Space Science
University of California at San Diego
La Jolla, California 92093

23. Dr. J. Hyman 1
Hughes Research Lab
3011 Malibu Canyon Road
Malibu, California 90265

24. Dr. T. Williamson 1
Hughes Research Lab
3011 Malibu Canyon Road
Malibu, California 90265

25. Dr. S. Shawhan 1
NASA Headquarters/E
Washington, DC 20546

26. Dr. C. K. Purvis 1
MC 302-1
NASA Lewis Research Center
21000 Brookpark Road
Cleveland, Ohio 44135

27. Mr. M. Patterson 1
Low Thrust Propulsion Branch
NASA Lewis Research Center
21000 Brookpark Road
Cleveland, Ohio 44135

28. Mr. J. Kolecki — 1
MC 302-1
NASA Lewis Research Center
21000 Brookpark Road
Cleveland, Ohio 44135

29. Dr. C. R. Chappell — 1
NASA Marshall Space Flight Center
Huntsville, Alabama 35812

30. Dr. T. E. Moore, ES53 — 1
NASA Marshall Space Flight Center
Huntsville, Alabama 35812

31. Mr. Paul Craven — 1
NASA Marshall Space Flight Center
Huntsville, Alabama 35812

32. Ms. B. Giles — 1
NASA Marshall Space Flight Center
Huntsville, Alabama 35812

33. Dr. D. Ga'lagher — 1
NASA Marshall Space Flight Center
Huntsville, Alabama 35812

34. Dr. D. Reasoner — 1
NASA Marshall Space Flight Center
Huntsville, Alabama 35812

35. Dr. J. Burch — 1
Southwest Research Institute
P. O. Drawer 28510
San Antonio, Texas 78284

36. Dr. J. H. Waite — 1
Southwest Research Institute
P. O. Drawer 28510
San Antonio, Texas 78284

37. Dr. D. Hastings — 1
Department of Aeronautics and Astronautics
Massachusetts Institute of Technology
Cambridge, Massachusetts 02139

38. Dr. I. Katz — 1
S - Cubed
P. O. Box 1620
La Jolla, California 92038-1620

39. Dr. M. Mandell 1
S - Cubed
P. O. Box 1620
La Jolla, California 92038-1620

40. Dr. V. Davis 1
S - Cubed
P. O. Box 1620
La Jolla, California 92038-1620

41. Dr. J. Raitt 1
CASS
Utah State University
Logan, Utah 84322

42. Captain D. Allred 1
HQ, DNA/RAEV
6801 Telegraph Road
Alexandria, Virginia 22310

43. Professor Nobuki Kawashima 2
Institute of Space and Astronautical Science
Komaba 4 - chome
Meguro - ku
Tokyo, Japan 153

44. Professor W. Riedler 1
Institute fur Weltraumforschung Oesterreichische
Akademieder Wissenschaften
Inffeldgasse 12
A - 8810 Graz, Austria

45. Dr. K. Torkar 1
Institute fur Weltraumforschung Oesterreichische
Akademieder Wissenschaften
Inffeldgasse 12
A - 8810 Graz, Austria

46. Dr. R. Schmidt 1
Space Science Department
ESA/ESTEC
Noordwijk, The Netherlands

47. Dr. Arne Pedersen 1
Space Science Department
ESA/ESTEC
Noordwijk, The Netherlands

48. Dr. W. F. Denig — 1
Space Physics Division
Air Force Geophysics Laboratory/PHG
Hanscom AFB, Massachusetts 01731

49. Dr. N. Omidi — 1
IGPP
University of California at Los Angles
Los Angeles, California 90024

50. Dr. Maha Ashour - Abdalla — 1
IGPP
University of California at Los Angles
Los Angeles, California 90024

51. Lt. Paul W. Werner — 4
1309 Parsons, NE
Albuquerque, New Mexico 87112

52. Dr. T. L. Aggson — 1
Mail Code 696
NASA/GSFC
Greenbelt, Maryland 20771

53. Dr. J. McCoy — 1
Code SN3
NASA/JSC
Houston, Texas 77058

54. Dr. Mario Acuna — 1
NASA/GSFC
Greenbelt, Maryland 20771

55. Dr. J. Slavin — 1
NASA/GSFC
Greenbelt, Maryland 20771

56. Dr. Paul Wilbur — 1
Dept. of Mechanical Engineering
Colorado State University
Ft. Collins, Colorado 80523